The top-of-atmosphere, surface and atmospheric cloud radiative kernels based on ISCCP-H datasets: method and evaluation

Yuanchong Zhang[1], Zhonghai Jin[2], and Monika Verma Sikand[3]

[1]SciSpace LLC and NASA GISS
[2]SSAI, Inc. and NASA Langley Research Center
[3]Bronx Community College, CUNY

November 24, 2022

Abstract

This study aims to create observation-based cloud radiative kernel (CRK) datasets and evaluate them by direct comparison of CRK and the CRK-derived cloud feedback datasets. Based on the International Satellite Cloud Climatology Project (ISCCP) H datasets, we calculate CRKs (called ISCCP-FH or FH CRKs) as 2D joint function/histogram of cloud optical depth and cloud top pressure for shortwave, longwave, and their sum, Net, at the top of atmosphere (TOA), as well as, for the first time, at the surface (SFC) and in the atmosphere (ATM). All the FH CRKs are physically plausible. The direct comparison shows that FH agrees reasonably well with three other TOA CRK datasets. With cloud fraction change (CFC) datasets of the same histogram for doubled-CO_2 simulation from 10 CFMIP1 models, we derive all the TOA, SFC and ATM cloud feedback using the FH CRKs. Our TOA cloud feedback is highly similar to the previous counterparts. Based on the comparison for the 4 CRK datasets and the 10 CFC datasets, we estimate the uncertainty budget for the CRK-derived cloud feedback, which shows that the CFC-associated uncertainty contributes $> 98.5\%$ of the total cloud feedback uncertainty while CRK's is very small. Our preliminary evaluation also shows that some near-zero/small cloud feedback in the TOA-alone feedback indeed results from the compensation of sizable cloud feedback of the SFC and ATM feedback, demonstrating how the SFC- and ATM-CRK derived cloud feedback can be valuable in revealing some significant surface and atmospheric cloud feedback whose sum appears insignificant in TOA-alone feedback.

Hosted file

`zhang_etal_kernel-1b_z3_si_jgr-formatted.docx` available at https://authorea.com/users/527312/articles/602746-the-top-of-atmosphere-surface-and-atmospheric-cloud-radiative-kernels-based-on-isccp-h-datasets-method-and-evaluation

The top-of-atmosphere, surface and atmospheric cloud radiative kernels based on ISCCP-H datasets: method and evaluation

Yuanchong Zhang[12†], Zhonghai Jin[2] and Monika Sikand[3]

[1]SciSpace LLC, 2880 Broadway, New York, NY 10025, USA.

[2] NASA Goddard Institute for Space Studies, 2880 Broadway, New York, NY 10025, USA.

[3] Deptment of Engineering, Physics, and Technology, Bronx Community College, CUNY, NY, 10453, USA.

Corresponding author: Yuanchong Zhang (yz7@columbia.edu)

Key Points:

- The cloud radiative kernel datasets are created for longwave, shortwave and their sum, net, respectively, at the top of atmosphere, the surface and in the atmosphere, of which the top-of-atmosphere cloud kernels are evaluated by direct comparison with the counterparts of other three datasets. In addition, our top-of-atmosphere cloud kernel derived cloud feedback is compared with the previous ensemble results from 10 climate models. Both comparisons show reasonably good agreement with the other counterparts.
- Uncertainty budget for cloud kernel derived cloud feedback at the top of atmosphere is estimated based on uncertainties of cloud kernels and cloud fraction change from the said comparisons. It shows that the cloud fraction change associated uncertainty contributes > 98.5% of the total cloud feedback uncertainty while cloud kernels' is very small.
- Our preliminary evaluation also shows that some near-zero or small cloud feedback in the top-of-atmosphere-alone feedback indeed results from the compensation of sizable cloud feedback of the surface and atmospheric feedback, demonstrating how the surface and atmospheric cloud kernel derived cloud feedback can be valuable in revealing some significant surface and atmospheric cloud feedback whose sum appears insignificant in the top-of-atmosphere-alone feedback.

Abstract

This study mainly aims to create observation-based cloud radiative kernel (CRK) datasets and evaluate them by direct comparison of CRK and the CRK-derived cloud feedback datasets. Based on the International Satellite Cloud Climatology Project (ISCCP) H datasets, we use the ISCCP flux production code to calculate CRKs (called ISCCP-FH or FH CRKs) as 2D joint function/histogram of cloud optical depth and cloud top pressure for shortwave, longwave, and their sum, Net, at the top of atmosphere (TOA), as well as, for the first time, at the surface (SFC) and in the atmosphere (ATM). All the FH CRKs are physically plausible. The direct comparison shows that FH agrees reasonably well with three other TOA CRK datasets. With cloud fraction change (CFC) datasets of the same histogram for doubled-CO_2 simulation from 10 CFMIP1 models, we derive all the TOA, SFC and ATM cloud feedback using the FH CRKs. Our TOA cloud feedback is highly similar to the previous counterparts. Based on the comparison for the 4 CRK datasets and the 10 CFC datasets, we estimate the uncertainty budget for the CRK-derived cloud feedback, which shows that the CFC-associated uncertainty contributes > 98.5% of the total cloud feedback uncertainty while CRK's is very small. Our preliminary evaluation also shows that some near-zero/small cloud feedback in the TOA-alone feedback indeed results from the compensation of sizable cloud feedback of the SFC and ATM feedback, demonstrating how the SFC- and ATM-CRK derived cloud feedback can be valuable in revealing some significant surface and atmospheric cloud feedback whose sum appears insignificant in TOA-alone feedback.

Plain Language Summary

(optional)

1 Introduction

The notion of feedback is referred to internal, mutually interacting processes in nature and was introduced to climate literature in 1960s (Manabe, 1969). In the past two decades, the radiative kernel technique has become a useful tool in studying climate feedback (Shell et al., 2008). A climate radiative kernel represents a differential radiative response to a climate variable's change from a reference (control) state. For climate feedback, usually the change of the net radiative flux effect (or forcing) at the top of atmosphere (TOA), $\Delta(Q - F)$, is concerned, where Q is the absorbed shortwave (SW) radiation by the atmosphere-earth system and F is outgoing longwave (LW) radiation (OLR) (Soden et al., 2008). With assumption that no interactions or nonlinear responses among the various climate processes are permitted, we may describe the radiative kernel approach for climate feedback using,

$$\gamma = \frac{\Delta(Q-F)}{\Delta T_s} = \sum_i \frac{\partial(Q-F)}{\partial X_i}\frac{dX_i}{dT_s} = \sum_i K_{x_i}\frac{dX_i}{dT_s} = \sum_i \gamma_i \qquad (1)$$

where, γ is the total climate feedback, the sum of individual feedback terms, γ_i, which may be decomposed into two parts, the radiative kernel, $K_{x_i} = \frac{\partial(Q-F)}{\partial X_i}$, the rate change of the TOA net flux with respect to climate variable, X_i, and, $\frac{dX_i}{dT_s}$, the rate of change of the climate variable, X_i, with respective to T_s, the surface air temperature. This separation facilitates climate feedback estimate because radiative kernels are usually calculated offline based on mean climate state and relatively insensitive to a particular mean climate state, compared to the intermodal differences in climate response (Soden et al., 2008). When a non-cloud climate variable's rate of change, $\frac{dX_i}{dT_s}$, is available, its feedback can readily be obtained from the product of $K_{x_i}\frac{dX_i}{dT_s}$.

However, the above kernel approach cannot simply be applied to cloud radiative kernel (CRK) and cloud feedback because of their high nonlinearity with respect to cloud properties. Cloud feedback has traditionally been estimated through the partial radiative perturbation (PRP) method, "cloud forcing" analysis approach and the online feedback suppression approach (Bony et al., 2006). Soden and Held (2006) used the "residual" method and later Soden et al. (2008) used the "adjusting" method to indirectly estimate cloud feedback using non-cloud radiative kernels (for atmospheric temperature and humidity, water vapor, surface albedo, etc.). The cloud radiative kernel was not explicitly created and directly used in estimating cloud feedback until

Zelinka et al. (2012, thereafter Z2012) introduced 49 cloud types (bins) in defining and calculating CRK and cloud feedback based on 7 x 7 2D joint function/histogram of cloud optical depth (τ, as X) and cloud top pressure (CTP, as Y, see Fig. 1). The histogram is modified from the original 6 x 7 τ-CTP histogram, used in the International Satellite Cloud Climatology Project (ISCCP) (Rossow and Schiffer, 1999). The Z2012's method may be taken as a kind of linearization on τ and CTP for the CRK approach in estimating cloud feedback using $K_{x_i}\frac{dX_i}{dT_s}$, where X_i is cloud change of each of all the 49 cloud types (bins). Note that Chen et al. (2000) introduced and calculated "overcast cloud change flux" that has the same physical definition as the CRK but for a coarser (3 X 3) τ-CTP histogram and without introducing the notion of 'cloud radiative kernel'.

Since then, there have appeared a number of literatures (Yue et al., 2016; Zhou et al., 2013 and Berry et al., 2019) using Z2012's method to produce CRKs, with which to estimate cloud feedback. The CRKs may be GCM based, observation based or their combination. As the Cloud Feedback Model Intercomparison Project (CFMIP) Observation Simulator Package (COSP) software (Bodas-Salcedo et al. 2011) is implemented in GCMs, using COSP-ISCCP simulated cloud changes on CTP-τ histogram with CRKs has become a feasible tool for (directly) estimating GCMs' cloud feedback.

In this study, we focus on the calculation and evaluation of our cloud radiative kernels with their derived cloud feedback. Section 2 describes the method for calculating the CRKs based on the ISCCP H-series (ISCCP-H) products (Young et al. 2018) for both TOA and surface (SFC), and their differences, atmosphere (ATM). Section 3 describes features of the TOA, SFC and ATM CRKs. Section 4 compares the ISCCP-H based TOA CRKs and three other TOA CRK sets for evaluating our TOA CRKs as well as estimating uncertainties of TOA CRKs. Section 5 estimates the TOA cloud feedback uncertainty budget based on the uncertainties of CRKs and cloud fraction change (CFC) from GCMs. Section 6 describes and evaluates the TOA, SFC and ATM cloud feedback results derived using our CRKs and reports the preliminary findings from this study. Section 7 summarizes this study and draws conclusions.

Figure 1

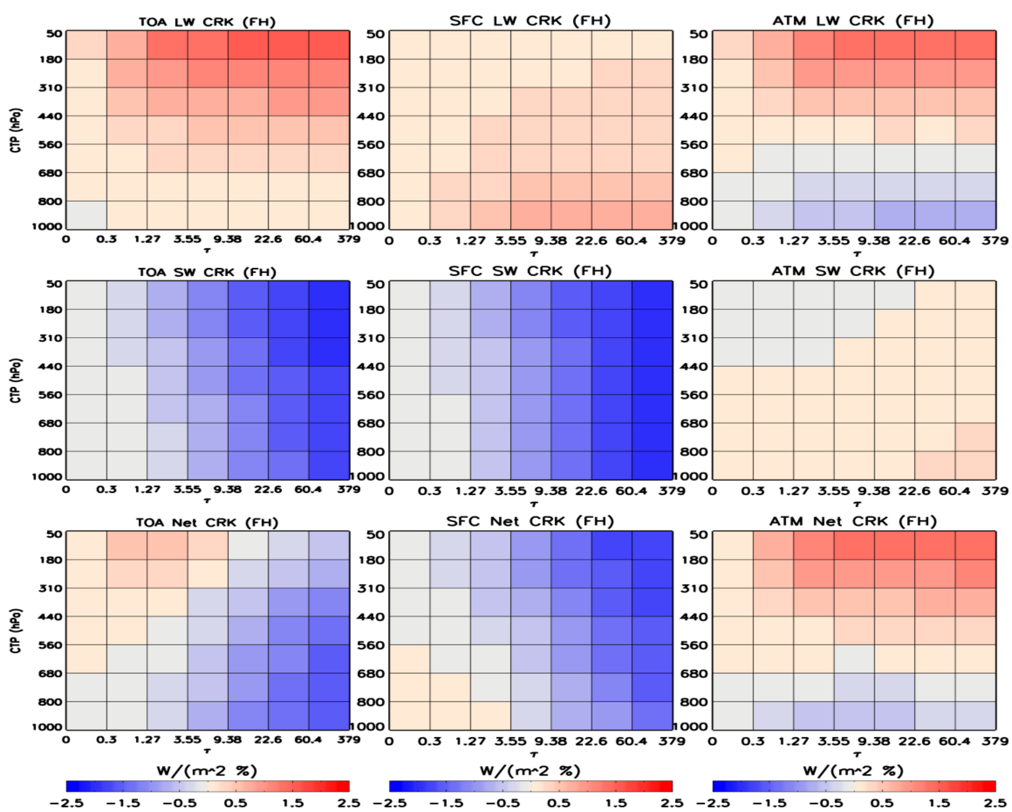

Fig. 1. Global, annual mean cloud radiative kernels, calculated using the ISCCP-FH code, for 49-bin histogram: the three (left to right) columns are for TOA, surface (SFC), and in atmosphere (ATM), respectively, and three (top to bottom) rows are for LW, SW and Net, respectively, in Wm^{-2} $\%^{-1}$.

2 Method to calculate cloud radiative kernels.

We use the ISCCP-FH flux production code to calculate our cloud radiative kernels (called ISCCP-FH or FH CRKs). The code has been used to produce radiative profile fluxes in 3-hourly on 110-km equal-area map for 1983 to 2017 (Zhang et al., 2021). It is modified from the radiation code of the GCM of the NASA Goddard Institute for Space Studies (GISS), ModelE2 (Schmidt et al., 2006), and it is equivalent to the radiation code of ModelE2.1 (Kelley et al., 2020). The ISCCP-FH radiation code is designed to be detailed, self-consistent and as realistic as possible, in which, SW and LW are all treated using the correlated k-distribution method and the atmospheric and surface properties are from consistent data sources. It has an accuracy of 1 Wm^{-2} for cooling rates (in degree/day) throughout the troposphere and most of the stratosphere (Lacis and Oinas, 1991) for LW and close to 1% for SW. The main input datasets for the ISCCP-FH code are from ISCCP-H products (Young et al. 2018). Through 1-yr, monthly and (110 km) regional comparison with the Clouds and the Earth's Radiant Energy System (CERES, Wielicki et al., 1996) and the Baseline Surface Radiation Network (BSRN, Ohmura, 2014) observations for TOA and surface, respectively (Zhang et al., 2021), it shows that the uncertainties are $\leq$ 10 Wm^{-2} at TOA and $\leq$ 20 Wm^{-2} at surface for the monthly, regional mean ISCCP-FH fluxes, which is slightly better than its precursor, the ISCCP-FD products (Zhang et al., 2004), but the former has higher spatial resolution of 110 km than the latter's 280 km.

For CRK calculation, the only major change of the code is that the ISCCP-H's (up to) 18 types of clouds are now replaced by 49 individual types of clouds as appearing in the 49-bin histogram (Fig. 1) with the specified CTP, τ and cloud amount (as defined in Z2012). All the other input parameters remain the same as those used in the ISCCP-FH flux production. Specifically, temperature/humidity profiles, surface properties (visible albedo, skin temperature) and snow/ice data are from the ISCCP-H datasets. The daily total solar irradiance (TSI) is based on the Solar Radiation and Climate Experiment (SORCE, V-15) datasets, equivalent to that used in CERES. Aerosol data is from Max Planck Institute Aerosol Climatology, version 2 (MAC-v2, Kinne et al., 2019). All the gases are the same as ModelE2's except ozone that is also from ISCCP-H. Clouds are specified as overcast (100% cover) in order to produce overcast cloud radiative effects (OCRE), for which the overcast-sky net flux replaces the original, all-sky net flux in conventional CRE (defined as the net flux difference between all sky and clear sky). The OCRE is calculated for SW, LW and their sum, Net (total), respectively, at TOA and surface for TOA and SFC CRK, respectively. For each of the 49 bins, the radiatively linearly, mid-values of CTP- and τ-bin ranges are used, which can be obtained by using ISCCP's counts-physical conversion table for pressure (CTP) and τ (Young et al, 2018; Rossow et al, 1996), so it is equivalent to Z2012's each bin's 4-corner flux average (but we only need to calculate once for a bin). The model sets the ISCCP-H's original relative humidity to 100% for cloud layers for (overcast) cloudy scene. Cloud particle sizes for liquid and ice are based on climatology from Han et al. (1994 and 1999). The ice phase in a cloud layer is defined when the temperature at CTP and cloud base are < 260 K and < 273.15 K, respectively; otherwise, the model sets to the liquid clouds. The cloud vertical structure used in the ISCCP-FH production is turned off as single-layer clouds are now used in consistency with the usage of the COSP-ISCCP simulation. The cloud thickness (therefore cloud base) is a function of cloud optical thickness τ, longitude, latitude, ocean/land, and month, based on a combination of the 20-year rawinsonde climatology

(Wang et al., 2000) and 5-year climatology from the CloudSat and CALIPSO data products (Stephens, et al., 2002; Winker et al., 2003). Clear-sky fluxes are calculated by setting cloud fraction = 0 and $\tau = 0$, which only needs to be calculated once for each grid cell. In the calculation, the TOA CRK, $K_{x_i} = \frac{\partial(Q-F)}{\partial X_i}$, is separated into two terms, $\frac{\partial(-F)}{\partial X_i}$ for LW, and $\frac{\partial(Q)}{\partial X_i}$ for SW, respectively, and their sum is the Net CRK. The ∂X_i here is the cloud amount change. All the CRKs are divided by 100 so they become a differential change of OCRE with respect to 1% CFC, expressed in $Wm^{-2}\ \%^{-1}$. The TOA formula can be extended to the surface and atmosphere with the OCRE definition in a consistent way.

Both the TOA and SFC CRKs are directly calculated in 3-hourly on 110-km equal-area map for year 2007. We have also produced the ATM CRKs by differencing the TOA and SFC CRKs. To our knowledge, SFC and ATM CRKs have not been published at the time of writing (though non-cloud SFC and ATM radiative kernels have been produced in the past few years, e.g., Kramer et al., 2019). Note that the SFC and ATM CRKs are just the two components, decomposed from the TOA CRKs. The original 3-hourly and 110-km kernel data is averaged to monthly (and annual) means and regridded to 250-km equal-area map which is also replicated to 2.5° longitude x 2.0° latitude equal-angle map for the majority of GCM-related uses. This coarser version of the ISCCP-FH cloud radiative kernel datasets (DOI: 10.5281/zenodo.4677580) can be downloaded from https://zenodo.org/record/4677580#.YHDsaDwpCUk.

3 ISCCP-H based TOA, surface and atmospheric cloud radiative kernels.

Fig. 1 shows the global, annual mean FH CRKs for 49-type clouds (bins) on the 7 x 7 histogram (X = τ and Y = CTP) for (Left to Right) TOA, SFC, and ATM in 3 columns, respectively; each column is for (top to bottom) LW, SW and Net, respectively. Note that each bin's CRK value is calculated for that type of clouds alone as if the rest types of clouds are not present in a grid cell. For a better illustration, we plot Fig. 2a (2b) for the 7 rows (columns) of the Fig. 1's CRKs as 7 individual functions of τ (CTP) to represent Fig. 1's each panel's 2D function, CRK(τ,CTP), in the same matrix order, so we will not specify which panel of Fig. 2a or 2b is compared with the panel of Fig. 1 unless the two panels in comparison are not for the same panels in their own matrices.

Figure 2a.

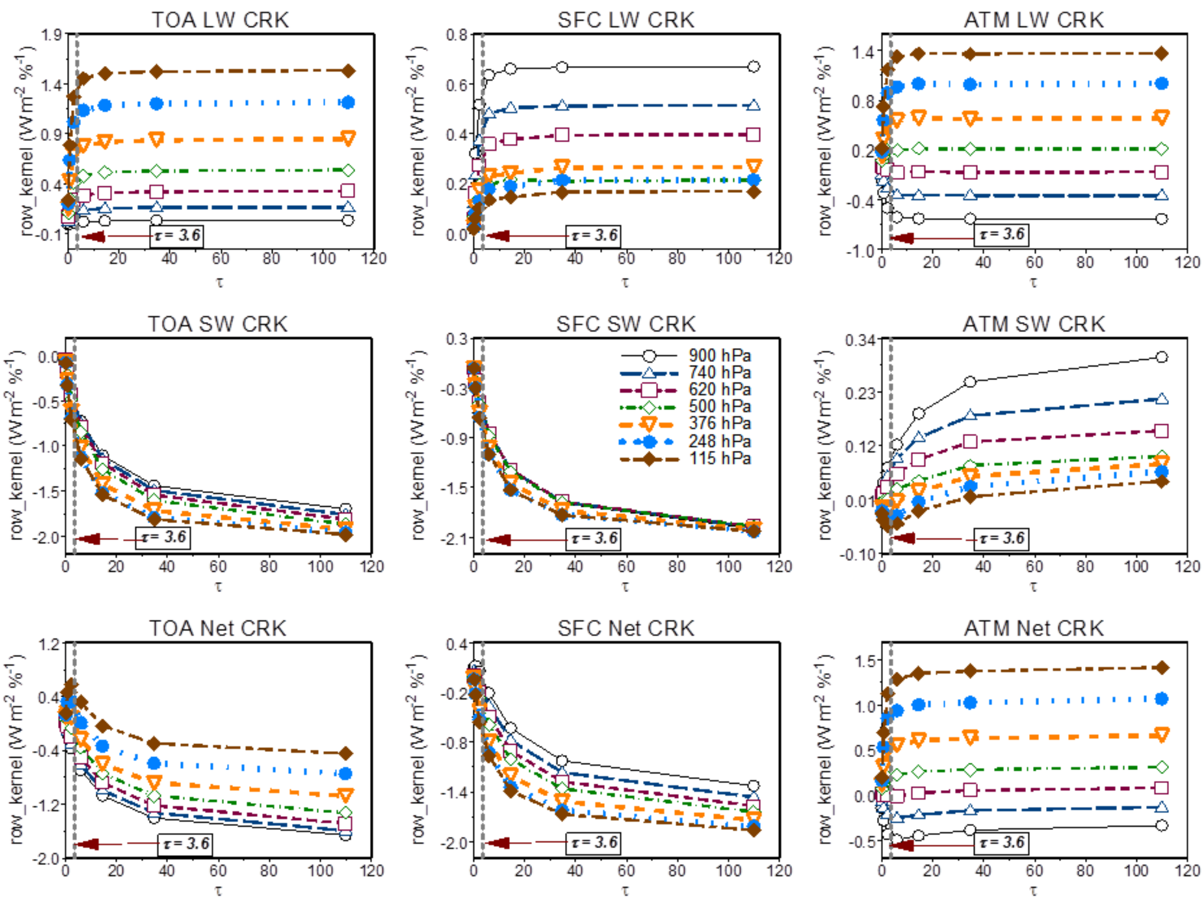

Fig. 2a. Seven rows of CRK (‘row_kernel’) of each panel of Fig. 1, as function of τ. The legend (central panel) shows radiatively linearly mid-level pressure of CTP layers for each row_kernel. The arrow indicates the vertical line of τ = 3.6.

Figure 2b.

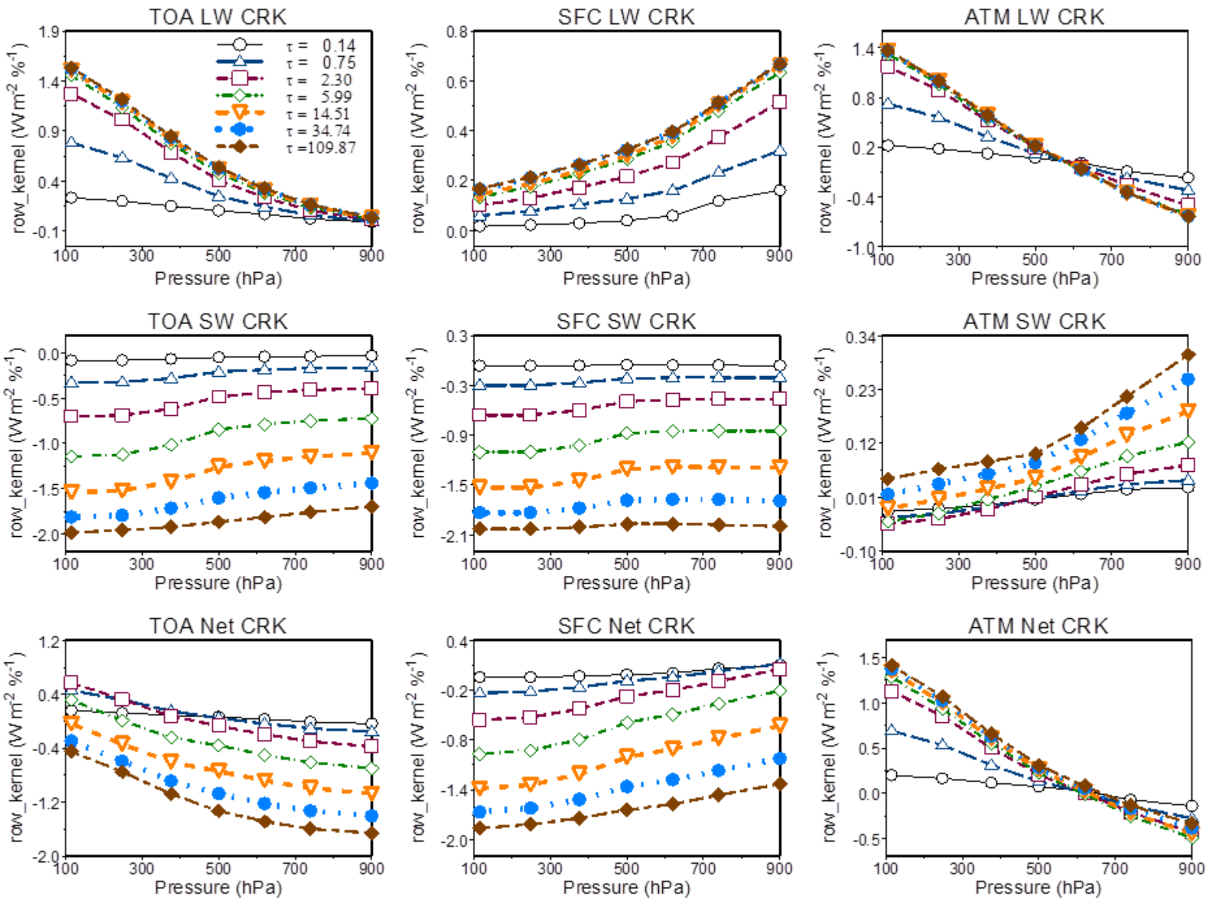

Fig. 2b. Seven columns of CRK ('col_kernel') of each panel of Fig. 1, shown as function of pressure. The legend (in top left panel) shows radiatively linearly mid-value of each column τ.

In Fig. 1, the 3 (left) TOA panels for LW, SW and Net CRKs are highly similar to the ensemble counterparts of (Fig. 1 of) Z2012, and the features described there have reappeared here, such as the LW CRK bins are all positive while all the SW CRK bins negative and LW CRK is sensitive to both τ and CTP for thin clouds ($\tau < 3.6$) but when τ 1≥ 3.6, LW CRK becomes insensitive to τ because of saturation (cf. Fig. 2a). We do not repeat what has been described in Z2012 but emphasize the following. 1The TOA LW CRK essentially depends on how much the surface emission (to TOA) is blocked by clouds, in which CTP has a dominant role while τ has a secondary role (especially when τ 1$\gtrsim$ 3.6), showing a generally horizontal layered structure (cf. Fig. 2a). In contrast to LW, the SW CRK's magnitude (in negative) essentially depends on how much TOA-incoming SW radiation is reflected by clouds, in which column τ has a dominant role while CTP plays a secondary role, showing a generally vertically layered structure (cf. Fig. 2b). As a result, the TOA Net panel shows their combined structure: roughly antisymmetric with respect to the diagonal line from the low left corner to the upper right corner; most of bins above (below) the line are positive (negative).

Fig. 1's middle column shows the SFC CRKs for (top to bottom) LW, SW and Net, respectively. The LW CRK panel shows that all the bins are also positive. The near-surface clouds most effectively block surface thermal emission (to the sky) and emit back so the largest SFC LW CRK values appear in the lowest cloud layer, somewhat like an upside-down of the TOA LW CRK panel but with magnitude reduced by ~1/2 (cf. Fig. 2a and 2b). The LW CRK decreases with CTP's decreases (increasing height) for each τ column, opposite to the TOA's (cf. Fig. 2a and 2b) because higher clouds block LW emission (from the surface) less effectively while having less emission to reach the surface (mainly because of lower temperature and water vapor). It also increases as τ increases for each CTP row before reaching $\tau \approx 3.6$ but then increase slowly (saturated, cf. Fig. 2a). The SFC SW panel is similar to the TOA's since column τ plays a dominant role for both of them (cf. Fig. 2b), and to a second degree, its magnitude also has small decrease with height (cf. Fig. 2b and 2a) since, for the incoming SW from space, the thicker τ is and the higher cloud layer is, the more SW is reflected back to TOA so the larger its SFC CRK is in magnitude (in negative). The SFC Net CRK panel seems somewhat like an upside-down of the TOA Net CRK panel and roughly appears antisymmetric with respect to the diagonal line from the upper left corner to the lower right corner; most of the bins above (below) the line are now negative (positive) (cf. Fig. 2a and 2b). The sign of each bin depends on the competition between LW and SW CRK values. Overall, SW outweighs LW, so all the bins have negative values except six bins at the low left corner for the SFC Net CRK.

The right column in Fig. 1 is for the ATM CRKs, determined by the difference between the TOA and SFC CRKs. The ATM LW CRK essentially depends on how much of the sum of upward surface emission and downward emission (from clouds and other atmospheric constituents) can possibly be absorbed by the atmosphere (including clouds) and it shows a generally horizontally-layered structure (cf. Fig. 2a) like the TOA and SFC' LW CRKs, indicating CTP's dominance. For the same τ column, the lower a cloud layer (bin) is, the more upward surface emission is blocked into the atmosphere and the less downward emission into the atmosphere from a cloud layer (but also compensated some by more downward emissions for near surface layers with higher temperature and humidity), and the less available LW flux that can possibly be absorbed by the atmosphere such that it becomes so small that is even smaller than the clear-sky atmospheric absorption, resulting in negative ATM LW CRK for near-surface clouds. This sign change is clearly shown in Fig. 2b: the cross point at pressure ≈1 600 hPa divides (right to left) negative-to-positive LW CRK values and when cloud layers go higher (smaller CTP) and pass the point, the LW CRK becomes positive. The saturation for τ 1≳ 3.6 is still present (cf. Fig. 2a). The ATM SW CRK is much smaller than both the TOA and SFC CRKs because they are largely cancelled (from their differencing). Physically, the ATM SW CRK depends on how much incoming SW flux is available for absorption by the atmosphere. For high clouds (CTP 1≲ 440 hPa) with $\tau < 22.6$, the majority of bins of clouds more or less block incoming solar fluxes from entering into the atmosphere so the total available SW flux is smaller than clear-sky's that causes negative CRKs (cf. Fig. 2a and 2b). This situation is changed when τ becomes thicker that causes more SW flux absorption by clouds (along with atmosphere), outweighing clear-sky absorption so the SW CRK becomes positive (cf. Fig.2a and 2b). For all the middle and low clouds (CTP 1≥ 440 hPa), more sunlight can enter into the atmosphere such that the SW absorbed by atmosphere and clouds becomes larger enough to outweigh clear-sky's atmospheric absorption, with its maxima appearing in the three lower right corner bins (cf. Fig. 2a and 2b). The (bottom) panel for ATM Net in Fig. 1 is the superposition of the above ATM LW and SW CRKs, of which, the former's magnitude is much larger than the latter, and, as a result, it is somewhat like ATM LW CRK, showing that almost all the high and middle clouds (CTP < 680 hPa) heat the atmosphere while the rest clouds have cooling effects on the atmosphere (cf. Fig. 2a and 2b).

All the features of the FH CRKs described above are qualitatively consistent with our observations and physical understanding for cloud radiative effects at TOA, surface and in atmosphere, reflecting self-consistency of the ISCCP-FH code and its input datasets from ISCCP-H.

4 Comparison of four TOA CRK datasets in evaluating FH CRKs.

As mentioned above, there are so far only TOA CRK datasets available in publication to our knowledge. To have a meaningful evaluation for the FH's TOA CRKs by direct comparison, we require a selected TOA CRK dataset to have a similar CTP-τ histogram for at least 12 monthly means for both SW and LW with global coverage. There seems only a very limited number of such datasets that satisfy the requirement. To our best knowledge, we have only found three other qualified TOA CRK datasets: (1) the one used in Z2012, shortened as 'MZ' (for Model-mean climate states based by Zelinka), (2) the one used in Zhou et al. (2013), whose mean state is from the European Centre for Medium-Range Weather Forecasts (ECMWF) Interim Re-Analysis (ERA-Interim) assimilation, shortened as 'OZ' (for semi-Observation-based by Zelinka), and (3) the initial release of the CERES FluxByCldTyp-Day/Month Ed4A products, shortened as 'CS' (Sun et al., 2019; CERES Science Team, 2020).

Table 1 shows the basic characteristics of the TOA CRK datasets from FH, CS, MZ and OZ. Both the MZ and OZ CRKs are zonal, monthly means in its original form, produced using the same Fu-Liou radiation code, but with different mean climate states as input. In their CRK calculation, single-layer clouds are inserted into the atmospheric column of the Fu-Liou radiative transfer model by setting liquid or ice water content to nonzero values at the level closest to the specified CTP for the cloud layer. Their LW and SW CRKs have values for all 49 bins. Their LW CRK may be directly replicated to all longitudes of a global map (i.e., independent of longitudes) but their SW CRK is also function of surface clear-sky albedo and must be mapped to a 2D global map using surface clear-sky albedo. For simplicity, we use the FH's surface clear-sky albedo for the mapping because it only makes minor differences if using the CERES' (or others) surface clear-albedo (Appendix B, Zelinka et al., 2012).

The CERES FluxByCldTyp products provide Terra and Aqua daytime 1°-regional gridded daily and monthly averaged TOA radiative fluxes and the associated Moderate Resolution Imaging Spectroradiometer (MODIS) derived cloud properties stratified by cloud optical depth and cloud effective pressure. The FluxByCldTyp products utilize only daytime (solar zenith angle < 82°) observations. The CS CRKs are provided for 42 cloud types demarcated by 6 cloud optical depth and 7 cloud effective pressure layer bins (Fig. 3). Their first τ-bin (of 0 – 1.27) covers the first 2 τ bins (0 – 0.3 – 1.27) of the 7 τ bins in all the other 3 CRK datasets because the CERES-MODIS cloud algorithm can effectively retrieve only the optical depths greater than 0.3. However, we have found that the CS CRKs' first bin indeed has a minimum $\tau \approx 0.05$ reported in the CS' monthly mean τ data (for 42 cloud types). In addition, the algorithm has an optical depth detection limit of ≤ 150. The CS CRKs also treats both the single layer and multi-layer portions of the upper level cloud as the upper layer cloud, in contrast to all the other 3 datasets based on single-layer clouds. The uncertainties for FluxByCldTyp products are not available, but the uncertainty for monthly 1°x1° regional 42 cloud-type and clear-sky SW and LW fluxes are expected to be > 6.2 Wm^{-2} and > 2.6 Wm^{-2}, respectively, based on several uncertainty causes (CERES Science Team, 2020).

To compare TOA CRKs for FH and the other 3 datasets on common ground, we make them have a common spatial resolution of 250-km equal-area map by re-gridding if necessary (Table 1). There are a total of 8252 grid cells on a full 250-km equal-area global map. Typically, the FH CRKs are virtually fully-mapped (only limited by highlands where low/middle cloud types cannot possibly exist as their CTPs may become underground). The longitudinally mapped MZ and OZ CRKs have values for 100% cells for all the 49 bins for LW, but ~97% for SW or Net (because FH's surface clear-sky albedo dataset has no data for polar nights in the SW mapping), implying that there may appear some unrealistic bins below ground level. The CS CRKs have only ~65% cells (of 42 bins) with data, under-sampled by ~1/3, but it is with real topography.

Fig. 3 shows global, annual mean TOA CRKs for 49-bin (42-bin for CS) histogram for MZ, OZ and CS, respectively. Together with Fig.1's left column for the FH's TOA CRKs, we can see that the 4 sets of TOA CRK are similar and they generally have all the features as described in Section 3.

Figure 3.

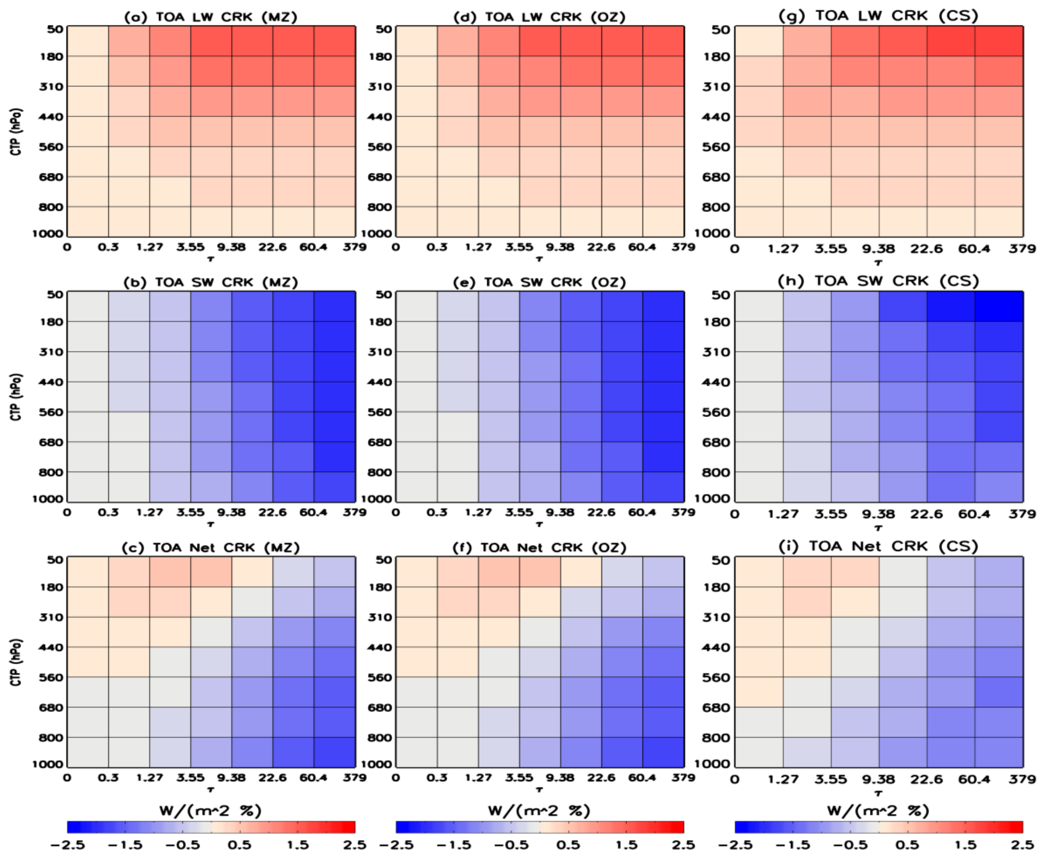

Fig. 3. Global, annual mean TOA cloud radiative kernels for 49-bin histogram (42 bins for CS) in Wm^{-2} $\%^{-1}$: (left to right) column s are for MZ, OZ and CS CRKs, respectively, and (top to bottom) rows are for LW, SW and Net CRKs, respectively.

To have a quantitative evaluation for FH and (in general) estimate uncertainties based on all the 4 sets for TOA CRKs, we make a statistical comparison for each of the 6 pairs that are all of the possible combinations of the 4 sets as shown in Table 2. From Table 2, we see that all the pairs have a high correlation (> 0.92), with an average of 0.96, 0.99 and 0.97 for LW, SW and Net, respectively. We also see much smaller mean differences (≤ 0.08) and standard deviation (Stdv ≤ 0.027) with the highest correlation (≥ 0.999) between the MZ and OZ CRKs, indicating that the 2 CRKs have relatively high similarities since they are calculated using the same Fu-Liou code even though their mean climate states are different and that CRKs are not sensitive to mean climate states . As we are not sure which of them represents 'absolute truth', we treat them as ensemble realizations of actual climate such that their differences represent an estimate of the uncertainty in their measurements or datasets (Zhang et al., 2006) without particular favor by using the modulus (absolute) mean difference (e.g., Reynolds, 1988). The modulus mean difference (Stdv) of the 6 pairs are 0.027 (0.122), 0.083 (0.130) and 0.064 (0.162) Wm^{-2} $\%^{-1}$ for LW, SW and Net, respectively. Their (bias included) RMS are 0.124, 0.154 and 0.174 Wm^{-2} $\%^{-1}$, which are our uncertainty estimate for monthly, regional (of 250 km, through the rest of text), cloud-type mean TOA CRKs for LW, SW and Net, respectively. As the MZ and OZ CRKs are not completely independent of each other (because the same Fu-Liou code is used for them), the above uncertainty estimates are probably underestimated. If we remove the OZ CRKs, and make the same comparison but for the rest 3 datasets (FH, MZ and CS) in all their possible 3 combinations (3 pairs), the RMS is increased by~20% (Table S1 in Supporting Information, SI), which may be more objective.

To explore more details in their differences, we partition τ to thin (τ < 3.55) and medium-to-thick (shortened as 'med-thick', for τ ≥ 3.55) and CTP to high (50 – 440 hPa), middle (440 – 680 hPa) and low (680 – 1000 hPa) clouds, and then make zonal means for each of the 6 sub-histograms for LW, SW and Net for FH, CS, MZ and OZ, respectively. To have a physically meaningful comparison, we strictly require the 4 CRK datasets to have data cells matched for all the bins on 250-km equal-area map. For a 7 x 7 histogram, its first two τ bins are required to have data in matching CS' first τ bin. Fig. 4a shows the comparison for zonal, annual means for high, middle and low clouds for LW, SW and Net, respectively, for thin-τ, and Fig. 4b is the same but for med-thick τ.

Figure 4a.

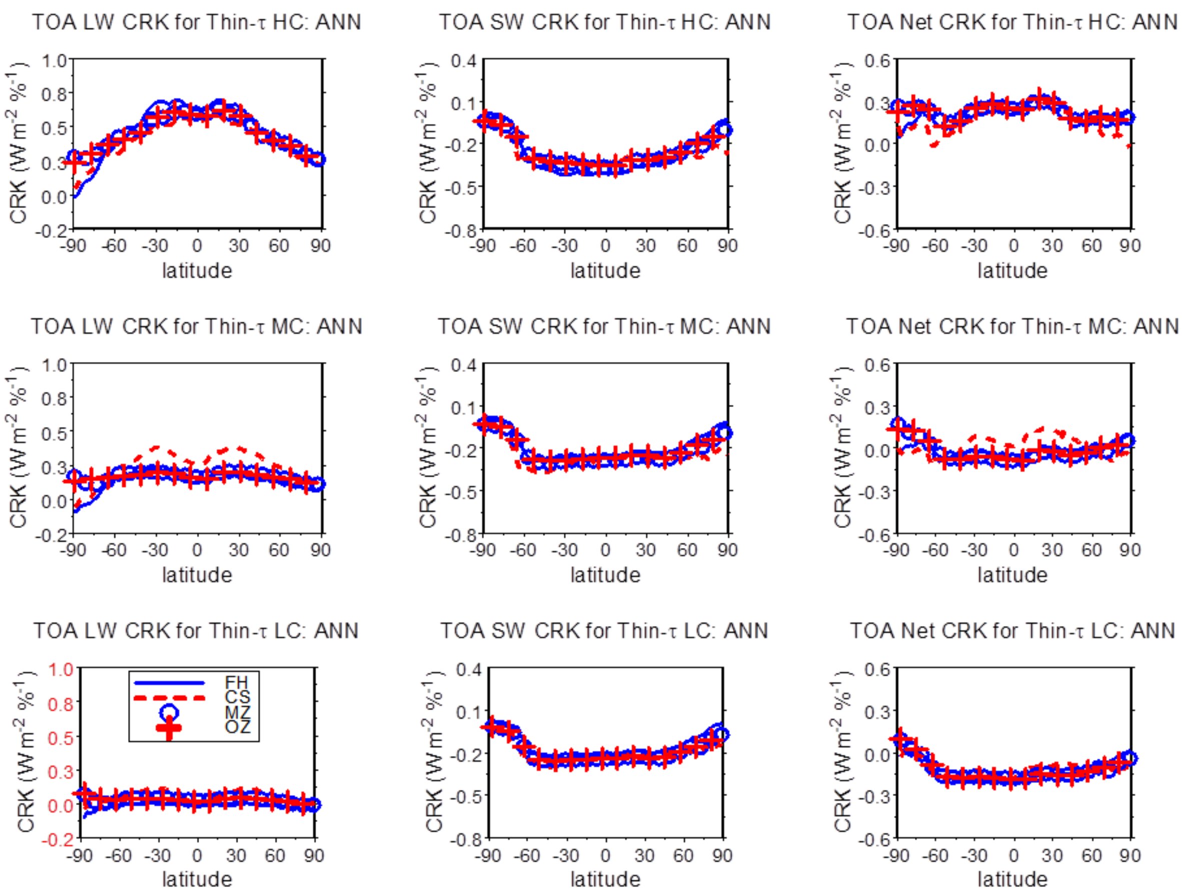

Fig.4a. Comparison of zonal, annual mean TOA cloud radiative kernels for thin τ (< 3.55) for FH, CS, MZ and OZ, respectively, for (top to bottom) high clouds (HC), middle clouds (MC) and low clouds (LC) and (left to right) LW, SW and Net, respectively.

Figure 4b.

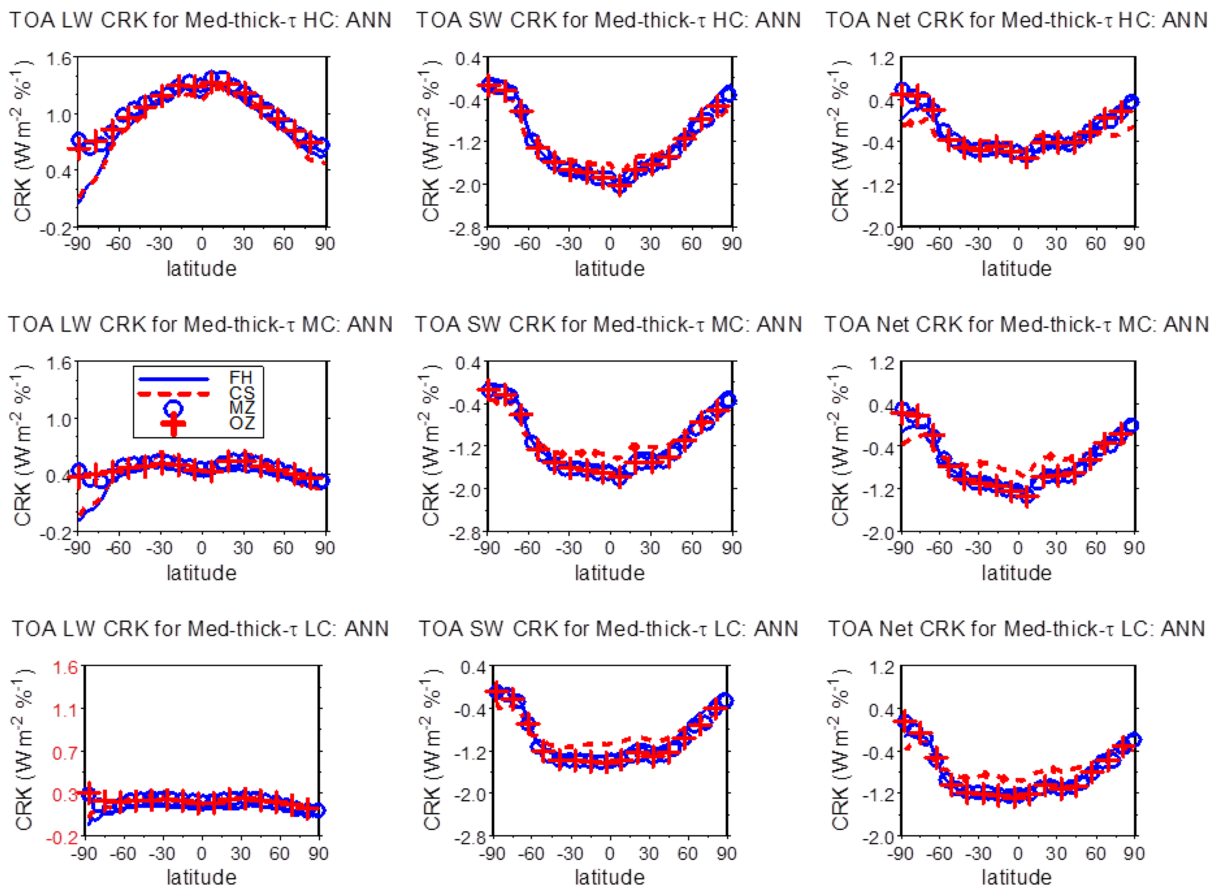

Fig. 4b. Same as Fig. 4a, but for medium-to-thick (‘Med-thick’) τ (1≥ 3.55) clouds.

Both figures 4a and 4b show that the 4 TOA CRK sets have a good agreement and their differences are generally within their uncertainty ranges, especially for SW in Fig. 4a. The LW CRKs have relatively larger zonal variations for high clouds than middle and low clouds that are relatively flat with the magnitude reduced substantially from high to low clouds as CTP has a dominant role for them. The mean magnitudes are roughly doubled from thin-τ to med-thick-τ. In contrasts to LW CRKs, the SW CRKs have similar zonal variations with magnitudes (in negative) slightly reduced from high to low clouds (as column τ is dominant). For SW CRK, the mean magnitudes of med-thick-τ (in negative) are about quintuple of that of thin-τ, much larger than LW CRKs' counterparts.

However, three local zonal areas appear to have large differences, exceeding the monthly, regional, and cloud-type mean uncertainty ranges (Table 2). First, over the south polar zones (poleward of ~75° S) , the LW CRKs of FH and CS are nearly coincident for both the thin τ and med-thick τ (Figures 4a and 4b) for all the high, middle and low clouds with magnitude lower than that of MZ and OZ which are also nearly coincident. The magnitude of the differences between the two pairs (FH/CS and MZ/OZ) varies with CTP and zone: decreases from high to low clouds and increases towards the South Pole. Its maxima appears at the South Pole, which can be as large as ~0.2 Wm^{-2} $\%^{-1}$ for thin τ and ~0.5 Wm^{-2} $\%^{-1}$, for med-thick τ, about double and quadruple of the RMS (0.124 Wm^{-2} $\%^{-1}$), respectively. Such differences between the two pairs may reflect the different natures between model-based and observation-based CRKs over Antarctic regions, where both observations and models have large uncertainties. They also reflect the difference in temperature/humidity profiles between FH and MZ/OZ since SW CRKs have no such differences in Antarctic zones. Second, over the subtropical latitudes around 30° for both the hemispheres, there appear up to 0.2 Wm^{-2} $\%^{-1}$ differences (nearly double the RMS) between CS and all the other 3 sets, but only for the thin-τ and middle clouds of LW CRK (Fig. 4a). As the subtropical zones are where cloudiness reaches minima (Peixoto and Oort, 1991), it is difficult for MODIS-CERES to have accurate retrievals when both of small cloud amount and thin τ (< 3.6) are present that may explain the wave-like outlies from CS. We have looked at the corresponding CS' zonal-mean cloud fraction (not shown) in the same fashion as Figures 4a and 4b (high, middle and low clouds for the two τ ranges), which shows that the cloud fraction over the said subtropical latitudes for middle clouds and thin-τ are very low, 1≲ 1%, while all the others are generally larger than 1% (except middle clouds with med-thick τ, for which it may become better for retrievals because of thicker τ). Third, over the tropical and subtropical zones (~45° S to ~45° N), the SW CS CRKs for med-thick τ (Fig. 4b), mainly for middle and low clouds, are larger than the other 3 sets with the difference of up to 0.4 Wm^{-2} $\%^{-1}$ around the equator, more than double of the SW CRK's RMS (0.154). After some investigation (e.g., overlapping cloud effects), we are unable to attribute such differences to any one single cause, but note that the peak of the difference appears in the equatorial belt of strong convections around the Intertropical Convection Zone (ITCZ) that may make it difficult for MODIS-CERES to have accurate retrievals for low and middle clouds.

In short, the FH TOA CRKs agrees reasonably well with the other three CRK datasets and all the four datasets of TOA cloud radiative kernels perform well. However, there are also a few of local zonal areas with relatively large differences of up to double of their RMS in general, and up to quadruple of the RMS in the extreme for the zones near the South Pole for LW CRKs where both the calculated and observed CRKs have large uncertainties.

5 Uncertainty budget of CRK-derived cloud feedback.

For evaluation on the FH CRKs using CRK-derived cloud feedback results, we use the ISCCP-simulated CFC results from 10 CFMIP1 models (Table 3), which are among the 11 models used in Z2012, but we drop one model because it has a quality issue (personal communication with Dr. Zelinka). We use the 10 CFMIP models' results because they are the best fit to our evaluation for direct comparison and we cannot find more relevant, similar results from modern CMP6/CFMIP3 results pertinent to our present purpose.

In the same fashion as done for CRK (Table 2), we have compared CFC from control run ($1 \times CO_2$) to $2 \times CO_2$ (equilibrium) run for a total of 45 pairs of all possible combinations for the 10 CFMIP1 models (normalized by surface air temperature). The modulus mean of the 45 pairs' mean difference (Stdv) is 0.004 (0.332) in $\%K^{-1}$, which is translated to RMS of 0.332 $\%K^{-1}$ that is our uncertainty estimate for CFC in monthly, regional, cloud-type means. For the details, see Table S2 in SI.

Given the uncertainties (RMS) of CRKs (Table 2) and CFC (Table S2 in SI), we can have a quantitative estimate on the uncertainty budget for cloud feedback. The CRK-derived cloud feedback is $K_{X_i} \frac{dX_i}{dT_s}$ (Section 1) with X_i for cloud amount. For simplicity, we rewrite it as $k \cdot \Delta C$, where k is our CRK (= K_{X_i}) that can be for LW, SW or Net, and ΔC is CFC (= $\frac{dX_i}{dT_s}$). Thus, the cloud feedback uncertainty may be estimated by its differential change, which can be decomposed into two terms with uncertainties (RMS) contributed by CRK and CFC, respectively, as shown in Eq. (2):

$$\delta(k \cdot \Delta C) = \delta k \cdot (\Delta C) + k \cdot \delta(\Delta C) \qquad (2)$$

where, the left side term is the total cloud feedback uncertainty, and the two right side terms, $\delta k \cdot(\Delta C)$ and $k \cdot\delta(\Delta C)$, are its decomposed ones, associated with the uncertainties contributed by CRK (k) and CFC (ΔC), respectively. The values of δk and $\delta(\Delta C)$ can be directly taken from their RMS while k and ΔC can be taken from the average of the absolute mean X and Y from Table 2 and Table S2 (in SI), respectively. Table 4 shows the uncertainty budget estimates for cloud feedback based on Eq. (2), which indicates that the cloud feedback uncertainty, $\delta(k\cdot\Delta C)$, is 0.177, 0.318 and 0.142 $Wm^{-2} K^{-1}$, for LW, SW and Net, respectively. Note that the CFC-uncertainty associated term, $k \cdot\delta(\Delta C)$, is 0.176, 0.316 and 0.140 $Wm^{-2} K^{-1}$, for LW, SW and Net, respectively, which contributes around two-order larger (> 98.5% of the total uncertainty) than the CRK-uncertainty associated term, $\delta k \cdot(\Delta C)$, which is respectively 0.0012, 0.0015 and 0.0017 $Wm^{-2} K^{-1}$. The uncertainty budget provides a statistical support of why cloud radiative kernel's uncertainty is less important compared with spread of GCM CFC uncertainty. The recent CMIP6 experiments show cloud feedback uncertainty of ~0.36 $Wm^{-2} K^{-1}$ (0.49 and 0.26 for SW and LW, respectively) in 1 Stdv, compared with CMIP5's of ~0.34 $Wm^{-2} K^{-1}$ (0.38 and 0.18 for SW and LW, respectively) (Zelinka et al., 2020b), which are comparable to our results, even though our results are based on the 10 CFMIP1 (CMIP3 era) models.

6 Preliminary TOA, SFC and ATM cloud feedback results derived using FH CRKs.

Based on the ISCCP-simulated cloud fraction change (CFC) from the 10 models, we can calculate cloud feedback at TOA, surface, and in the atmosphere. To our knowledge, the SFC and ATM cloud feedback that are directly derived from the SFC and ATM CRKs have not been previously published so our direct comparison of cloud feedback is restricted to TOA cloud feedbacks only, for which we use Z2012's results as they are relatively more comprehensive and relevant (based on about the same CFMI1 models' CFC results, Section 5). However, we also look at some overall characteristics of SFC and ATM cloud feedback in global and zonal means. Note that the SFC and ATM cloud feedback are the two components decomposed from the TOA cloud feedback (similar to the TOA CRK's decomposition).

Figure 5.

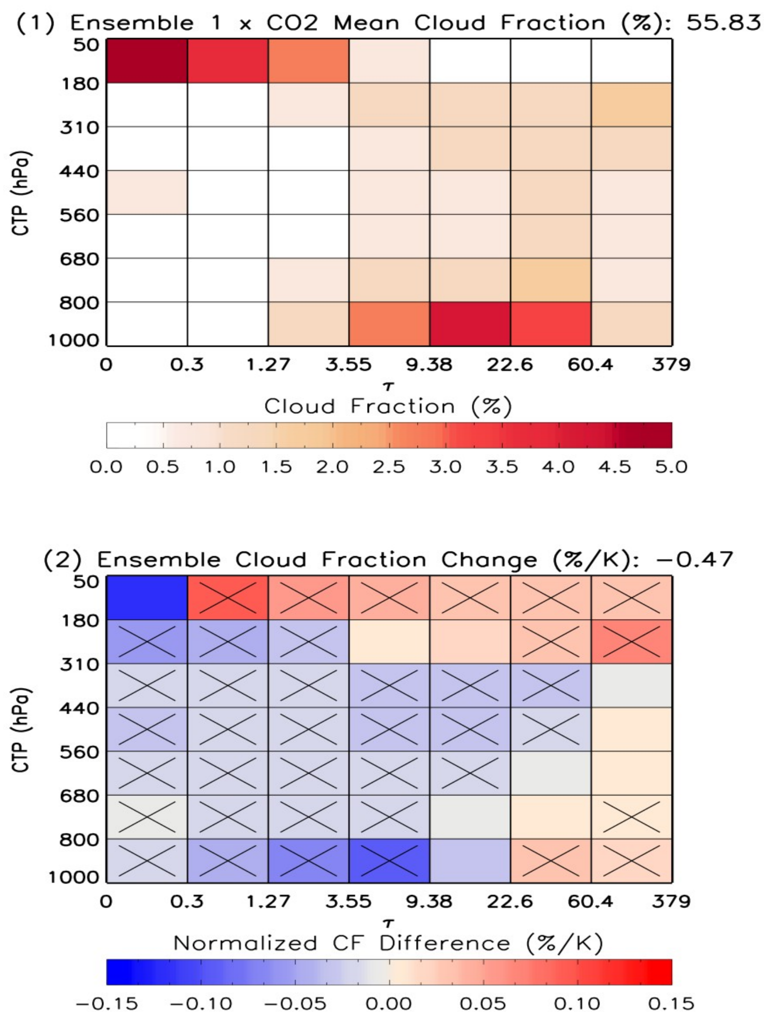

Fig. 5. Global, annual, 10 CFMIP1 model ensembled mean cloud fraction for 1 x CO_2 in (1),and cloud fraction changes from 2 x CO_2 runs, in (2), with respect to (1), normalized by the change of each model's global mean surface air temperature changes between the two states in % K^{-1}. A bin marked by 'x' indicates that 1≥ 80% of models agree on the sign of the bin. The sum of the 49 bins is shown in each title.

Fig. 5 shows global, annual and 10-model ensemble mean cloud fraction for 1 x CO_2 and CFC from 2 x CO_2 experiments. They are very close to Z2012's panels (a) and (c) of their Fig. 2 with slightly different total value (sum of 49 bins, shown in the titles) though we only use 10 of 11 of their models' data. In the lower panel, we also show cross signs ('x') for the bins with ≥ 80% of models having the same sign, which are identical to the Z2012's sign indicators (but theirs are for ≥ 75% of the 11 models). The CFC with large magnitude mainly appears in high clouds (CTP < 440 hPa) and near-surface clouds (CTP > 800 hPa). Most of the CFCs are negative (decrease of cloud amount) with the largest (in magnitude) of -0.12 %K^{-1}, about 1/4 of the total (-0.47 %K^{-1}), for CTP < 180 and thinnest τ ($\tau \leq 0.3$), but there also appear large positive bins in high clouds (CTP < 310) and near-surface clouds with thick τ (> 22.6). The CFC features are consistent with that double CO_2 experiments generally cause high clouds to shift upward and low clouds with thin-medium τ reduced.

Fig. 6 shows the cloud feedback histograms for global and annual ensemble mean based on the 10 models for (left to right) TOA, SFC and ATM and (top to bottom) LW, SW and Net cloud feedback. The TOA cloud feedback panels are highly similar to Z2012's (d), (e) and (f) of their Fig.2 (although our cloud feedback results are from completely independent FH CRKs with only 10 of their 11 CFMIP1 models used). The cross signs ('x') in the left column (with the same meaning as Fig. 5) generally agree with Z2012's with slight differences. Table 5 shows the range of the total cloud feedback for global and annual mean for LW, SW and Net at TOA, surface, and in the atmosphere along with their ensemble values. All the ranges between Table 5 and Z2012 are consistent. Note that Table 5 also tells that the model spread is large.

Figure 6.

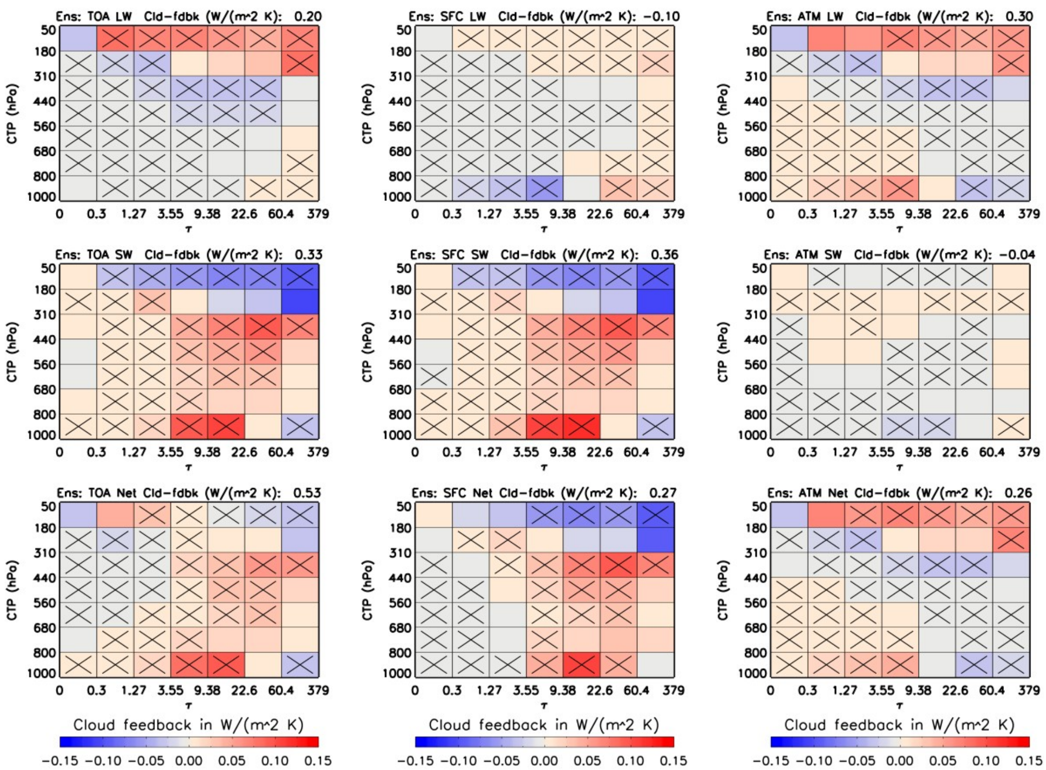

Fig. 6. Global, annual, ensemble ('Ens') cloud feedback for (left to right) TOA, surface and atmosphere for (top to bottom) LW, SW and Net, respectively. They are obtained by multiplying the (normalized) cloud fraction changes with FH CRKs for each bin, 250-km equal-area cell and month, and then average to global, annual, ensemble mean. A bin marked by 'x' indicates that 1≥ 80% of models agree on the sign of the bin. The sum of the 49 bins is shown in each title.

The (top middle) SFC LW cloud feedback of Fig. 6 shows that the majority of bins are negative with large-magnitude appearing in low clouds (1000 ≥ CTP > 800) among thin and medium τ range. Roughly, the near-surface clouds with thick τ, all bins with τ ≥ 60.4 and the majority of clouds with CTP < 310 are positive with several bins in large magnitude. Overall, the SFC LW cloud feedback has net cooling effects of -0.10 Wm^{-2} K^{-1}, about half of the TOA LW's (in magnitude). The SFC SW cloud feedback is similar to the TOA's (because their SW CRKs are similar, Section 3) with total feedback of 0.36 versus TOA's 0.33 Wm^{-2} K^{-1}. As the sum of the SFC LW's and SW's cloud feedback with the latter's dominance, the SFC Net cloud feedback shows that most of the high clouds (CTP < 310) have large cooling effects and the rest with medium and thick τ have larger heating effects on the surface that makes the total cloud feedback equal to 0.27 Wm^{-2} K^{-1}, about half of TOA Net's.

As the difference between TOA and SFC, large magnitude of the ATM LW cloud feedback mainly appears in high clouds and near-surface clouds. For high clouds of CTP < 180 hPa with $\tau > 0.3$, and $180 < CTP \leq 310$ with $\tau > 3.55$, clouds may block surface emission (to TOA) more effectively and emit back to the atmosphere (and surface) that makes more LW flux available for atmospheric constituents (including clouds) to absorb to heat atmosphere. For near surface clouds with thin-to-medium τ, they not only absorb a large amount of LW emission from surface, but also can leak certainty emission to the atmosphere that increases atmospheric absorption to have heating effects. For other clouds, cloud feedback's sign depends on how much LW flux can be available for the atmosphere to absorb. Overall heating is dominant so the total cloud feedback is 0.30 Wm^{-2} K^{-1}, although negative bins appear nearly half of all bins. The magnitude of the total ATM LW feedback (0.30) is equal to the sum of the magnitude of TOA (0.20) and SFC (-0.10) because both the increase of TOA cloud feedback and the decrease of SFC cloud feedback strengthen the ATM cloud feedback, which results in that cloud feedback of LW ATM is the largest of the three LW's feedback that may play an important role in modulating atmospheric circulation. The small ATM SW cloud feedback with a total of -0.04

$Wm^{-2} K^{-1}$, one order smaller than all the other (TOA, SFC and ATM) cloud feedbacks in magnitude, is mainly due to small ATM SW CRK. Because the majority of the ATM SW CRK bins are positive and the majority of CFC bins are negative, their product results in the majority (~2/3) of bins with a negative sign. The SW ATM cloud feedback seems the least important of all the cloud feedbacks. As sum of the ATM LW and SW cloud feedback, the Net ATM cloud feedback is overweighed by LW's since SW's is so small that the Net ATM cloud feedback is like a weak duplication of ATM LW feedback. The total Net feedback of ATM (0.26) is about half of the TOA's (0.53) with another half shared by the SFC's (0.27).

Fig. 7 shows the total cloud feedback (of 49 bins) for annual and ensemble mean on the global map for (left to right) TOA, SFC and ATM for (top to bottom) LW, SW and Net, respectively, based on CFCs from 4 models using the FH CRKs. All the LW, SW and Net cloud feedback features in the (left) TOA column are very similar to the left column of Fig. 5 in Z2012, though Z2012 uses 5 models, of which we dropped one because of a quality issue (personal communication with Dr. Zelinka). From Fig. 7, we can find some interesting features: (1) For LW cloud feedback, almost all the TOA's major features appear in the ATM LW cloud feedback (with the largest global mean for LW) except for both the polar regions where large surface heating appear in the SFC LW cloud feedback with much larger magnitude than both TOA and ATM LW feedback; (2) Although the global mean of the ATM SW cloud feedback is one order smaller than all the other cloud feedback's, the ATM SW has large heating effects in the atmosphere over polar regions while the SFC SW cloud feedback causes heating in the Amazon areas but cooling in the ~60° S belt; (3) For Net cloud feedback, the most noticeable is that the atmosphere of the ITCZ gets heating but that of the South Pacific Convergence Zone (SPCZ) gets cooling while the surface of the Amazon and the SPCZ gets heating but the ~60° belt gets cooling.

Figure 7.

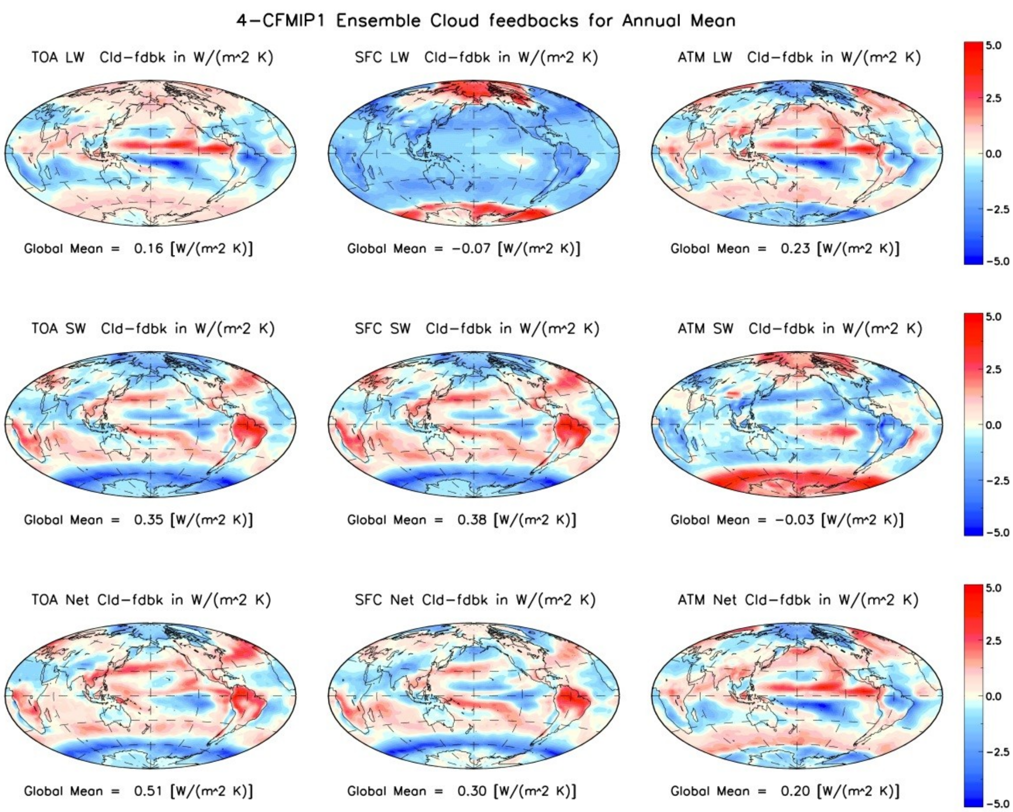

Fig. 7. Estimates of annual and 4-CFMIP1 ensemble mean cloud feedback for (left to right) TOA, SFC and ATM and (top to bottom) LW, SW and Net, respectively, derived using the FH CRKs. The left column is the same as the left column in Z2012's Fig. 5, which uses 5 CFMIP1 models: HadSM4, HadSM3, HadGSM1, MICRO (lowres) and AGCM4.0, of which the last is not used because of a quality issue (see footnotes in Table 3).

Fig. 8 shows zonal, (10-model) ensemble mean cloud feedback, partitioned into high, middle and low clouds for (left to right) TOA, SFC and in ATM for (top to bottom) LW, SW and Net, respectively, and (upper part of) Table 6 shows their respective global mean contributions.

The left column for the TOA cloud feedback seems like a duplication of the Fig. 6 in Z2012 (but only for 75° S to 75° N), even derived with the completely independent FH CRKs using only 10 of their 11 models. From the SFC and ATM feedbacks together with the TOA's, we can see some interesting features that may not appear in the TOA-alone feedback. First, Z2012 states that low cloud changes are irrelevant at all latitudes for the TOA LW cloud feedback as the low cloud feedback is nearly zero over all zones as shown in the (top left) TOA LW panel. However, with the SFC and ATM LW feedback available now, we see that the near-zero low cloud feedback in the TOA LW panel is indeed caused by the nearly entire compensation of the sizeable low cloud feedback between SFC and ATM. This is also reflected in their global average as shown in Table 6: TOA LW feedback for low clouds is only -0.01 but it is -0.07 and 0.06 $Wm^{-2} K^{-1}$ for SFC and ATM, respectively. Second, in the TOA Net cloud feedback, Z2012 states that because of their largely compensatory effects on the SW and LW cloud feedbacks, high cloud feedback contributes less than low cloud's to the net cloud feedback at all latitudes. With the SFC and ATM Net cloud feedback, we see that the high cloud feedback is indeed so large that it is comparable with the total feedback over most latitudes in the ATM Net cloud feedback, which is also largely compensated by the SFC Net's high cloud feedback so it seems small in the TOA Net cloud feedback, which is also reflected in their global average in Table 6.

Figure 8.

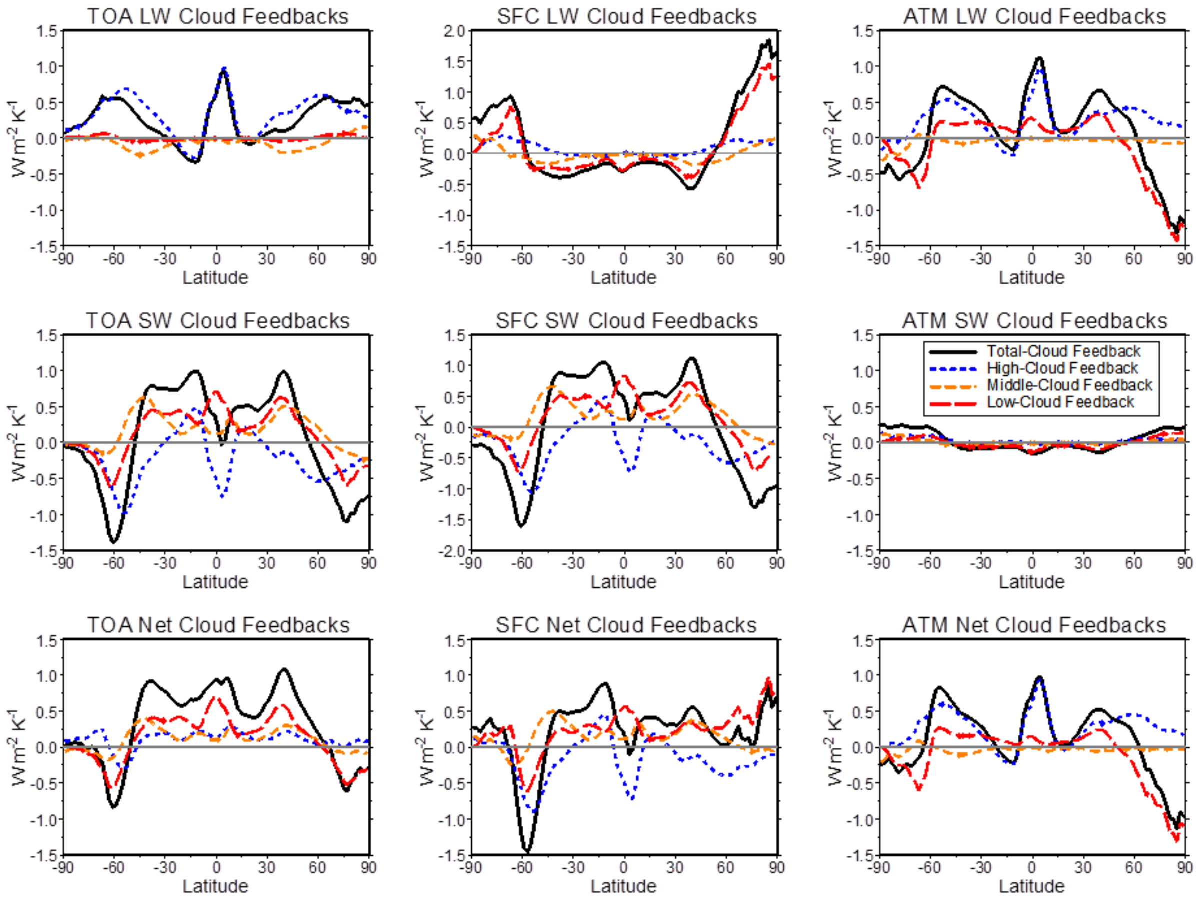

Fig. 8. Zonal, annual and (the 10-model) ensemble mean clod feedback, partitioned into high, middle and low clouds with their total for (left to right) TOA, SFC and ATM for (top to bottom) LW, SW and Net, respectively.

Fig. 9 is the same as Fig. 8 but the cloud feedback is partitioned into contributions from thin-, median- and thick-τ CFCs, and their global mean contributions are also shown in (lower part of) Table 6. The left column in Fig. 9 is also very similar to Fig. 7 in Z2012. We note that, for the LW cloud feedback, thin- and medium-τ feedback appear small but their SFC and ATM components are actually sizeable and their radiative effects cannot be overlooked, as also indicated in global average (Table 6).

Figure 9.

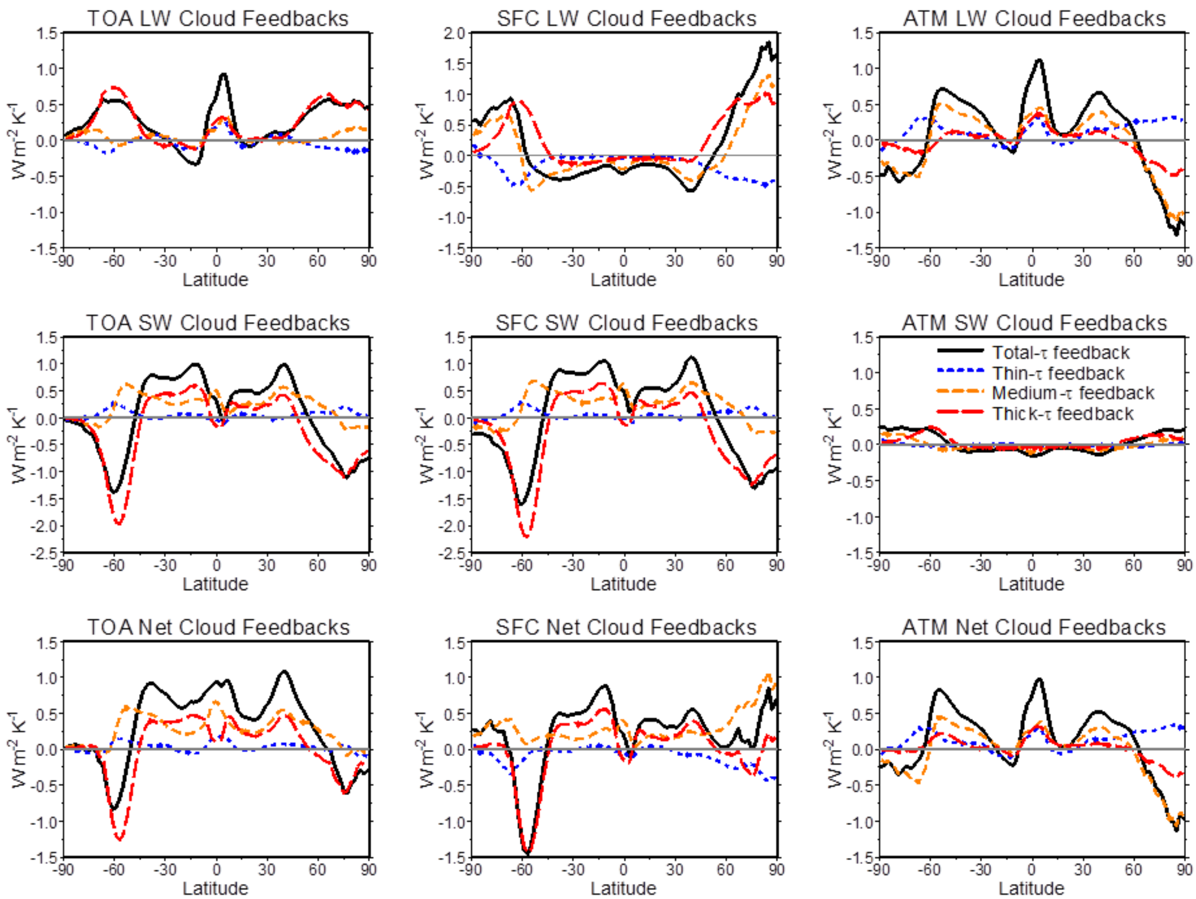

Fig. 9. Zonal, annual and (the 10-model) ensemble mean clod feedback, partitioned into thin, median and thick τ with their total for (left to right) TOA, SFC and ATM for (top to bottom) LW, SW and Net, respectively.

7 Summary and discussion.

The main purpose of this study is to create observation-based 2D cloud radiative kernels at TOA, surface and in the atmosphere and evaluate them by direct comparison with other CRKs as well as direct comparison of cloud feedback results between our CRK-derived and Z2012's counterparts. However, direct comparisons at present can only be conducted for TOA CRKs and its derived TOA cloud feedback because there are no available SFC and ATM CRKs and their directly derived cloud feedback datasets to our knowledge at the time of writing.

With the observation-based ISCCP-H datasets as inputs, we have used the ISCCP-FH profile flux production code to calculate the ISCCP-FH cloud radiative kernels at TOA, as well as, for the first time, at the surface and in the atmosphere for SW and LW, and their sum, Net, in 3-hourly on 110-km (and their replicated 250-km) equal-area maps, where the SFC and ATM CRKs are the two components decomposed from the TOA CRK's. By design, the FH cloud radiative kernels are as realistic as possible with self-consistency.

The FH TOA, SFC and ATM CRKs for LW, SW and Net (Fig. 1 and Fig. 2) show physically clear, overall quantitative pictures of OCRE imposed by 49 individual cloud types. The noticeable features of the CRKs are the CTP-dominant, horizontal-layered structure in all the LW CRKs and the column-τ dominant, vertical-layered structure in SW CRK histograms at TOA and SFC. The TOA and SFC Net CRKs show a roughly antisymmetric structure with respect to their diagonal line (in forward-slash and backslash direction, respectively). As the difference between the TOA and SFC CRKs, the LW and Net ATM CRKs show general heating (cooling) influence by high (low) clouds but only weak effects appear in the SW ATM CRK.

The comparison for the 4 TOA CRK datasets, FH, MZ, OZ and CS, shows that the FH CRKs agree reasonably well with the other 3 sets of CRKs, and that, in general, the 4 sets of CRKs perform well and their differences are within their uncertainty ranges. However, in their zonal means, there appear three locally large differences of up to double or so of their RMS, and, in extreme cases, up to quadruple of the RMS for the zones near the South Pole, where both the calculated and observed CRKs have large uncertainties. Therefore, given their different nature, the 4 sets of the TOA CRKs are more or less comparable in their practical usefulness though CS may somehow suffer under sampling that needs some caution in using it.

Moreover, through the comparison, we have estimated their uncertainties (RMS) as 0.124, 0.154 and 0.174 Wm^{-2} $\%^{-1}$, for LW, SW and Net, respectively, for (250-km) regional, monthly, cloud-type mean TOA CRKs. As the MZ and OZ CRKs are not completely independent of each other (because the same radiation code is used for them), the above uncertainty estimates are probably underestimated. If we remove the OZ CRKs, the RMS is increased by~20%, which may be more objective.

Before calculating CRK-derived cloud feedback, we have also estimated cloud fraction change uncertainty as 0.332 $\%K^{-1}$, based on 45 pairs of all possible combinations of the 10 CFMIP1 models' ISCCP-simulation for double CO_2 experiments. Combining uncertainties of CRKs and CFC with their means, we have estimated the uncertainty budget for the CRK-derived cloud feedback as 0.177, 0.318 and 0.142 Wm^{-2} K^{-1}, for LW, SW and Net, respectively, to which the CFC-associated uncertainty term contributes around two-order larger than that of the CRK-associated uncertainty term, accounting for > 98.5% of the total uncertainty. The implication is that the priority for improving cloud feedback accuracy is to have more accurate cloud fraction changes while CRKs are relatively accurate enough. Indeed, in viewing all the individual 10 models' CFC's global, annual mean matrixes, we see that they are very diversified (not show) that is also reflected in their ranges of their total global and annual means (Table 5) and their low correlation (of 0.13 in average, Table S2 in SI). The recent CMIP6 experiments show cloud feedback uncertainty of ~0.36 Wm^{-2} K^{-1} (0.49 and 0.26 for SW and LW, respectively) in 1 Stdv, compared with CMIP5's of ~0.34 Wm-^{2} K^{-1} (0.38 and 0.18 for SW and

LW, respectively) (Zelinka et al., 2020b). Both of the uncertainties are comparable with our above uncertainty values even though we use CFMIP1/CMIP3 era data.

We have shown that the cloud feedback derived from the FH's TOA CRKs is highly similar to Z2012's counterparts (figures 6, 7, 8 and 9 vs. the figures 2, 5, 6 and 7 in Z2012) though we use our completely independent CRKs with one model dropped from their original models used in Z2012. These comparisons have further verified the FH CRKs.

Although we cannot directly verify our SFC and ATM CRKs, they may be thought to be indirectly verified since our radiation code is self-consistent. In addition, our SFC and ATM cloud feedback show that the near-zero low cloud feedback for TOA LW is caused by the nearly entire compensation between the sizeable SFC and ATM LW cloud feedback, and that high cloud feedback contributes less than low cloud's to the net TOA cloud feedback at all latitudes is also largely compensated by the sizeable SFC and ATM Net's high cloud contribution so it seems small in the TOA Net cloud feedback. These are two examples to demonstrate how the SFC and ATM CRKs and their derived cloud feedback can be valuable in revealing what may possibly be significant in some hidden/insignificant cloud feedback in TOA-alone feedback, resulting from compensation of sizeable SFC and ATM feedback. The separated, significant SFC and ATM feedback may deepen our understanding in their individual influences on radiation, cloud feedback and general circulation that is not so obvious from the TOA-alone cloud feedback results. We will make a more detailed exploration of the SFC and ATM CRK-derived cloud feedback using the updated CMIP6 model results in a future study.

Acknowledgments, Samples, and Data

We are deeply indebted to Dr. Mark D. Zelinka who has contributed many valuable ideas as well as supplied his cloud radiate kernel and CFMIP1 datasets that make this paper possible. The CERES FluxByCldTyp-month data were obtained from the NASA Langley Research Center

CERES ordering tool at https:/ceres.larc.nasa.gov/data/. The ISCCP-FH cloud radiative kernel data was conducted on NOAA NCEI computer. This study is supported by the NASA MAP program (grant NNH10ZDA001N) and the NASA IDS program (award 19-IDS19-0059).

CERES FluxByCldTyp data can be ordered using DOI: 10.5067/Terra-Aqua/CERES/FLUXBYCLDTYP-MONTH_L3.004A. For Data Quality Summary, see https://ceres.larc.nasa.gov/documents/DQ_summaries/CERES_FluxByCldTyp_Ed4A_DQS.pdf.

The CFMIP1 model datasets and MZ (model based) CRK datasets are from the ones used in Zelinka et al. (2012). The OZ (ERA-Interim based cloud radiative kernels) CRK datasets are the ones used in Zhou et al. (2013).

The ISCCP-FH cloud radiative kernel in 2.5 longitude X 2.0 latitude can be downloaded from https://zenodo.org/record/4677580#.YHDsaDwpCUk. Its DOI is 10.5281/zenodo.4677580, which supplies both TOA and SFC CRKs for LW and SW, respectively, from which users can compute ATM CRKs (difference between TOA and SFC) as well as Net CRKs (sum of LW and SW) for all TOA, SFC and ATM.

References

Berry, E., Mace, G. G. & Gettelman, A. (2019). Using A-Train Observations to Evaluate Cloud Occurrence and Radiative Effects in the Community Atmosphere Model during the Southeast Asia Summer Monsoon, Journal of Climate, 32, 4145-4165, DOI: 10.1175/JCLI-D-18-0693.1.

Bodas-Salcedo, A., Webb, M., Bony, S., Chepfer, H., Dufresne, J., Klein, S., Zhang, Y., Marchand, R., Haynes, J., Pincus, R. &. John, V.O. (2011). COSP Satellite simulation software for model assessment, B. Am. Meteorol. Soc., 92, 1023–1043, https://doi.org/10.1175/2011BAMS2856.1, 2011.

Bony, S., & Dufresne, J. L. (2006). How Well Do We Understand and Evaluate Climate Change Feedback Processes? Journal of Climate, 19, 3445-3482.

CERES Science Team, (2020). CERES_FluxByCldTyp-Day/Month_Ed4A Data Quality Summary, https://ceres.larc.nasa.gov/data/.

Chen, T., Rossow, W. B. & Zhang, Y.-C. (2000). Radiative effects of cloud-type variations. J. Climate, 13, 264–286.

Fu, Q. & Liou, K. N. (1992). On the correlated k-distribution method for radiative transfer in nonhomogeneous atmospheres, J. Atmos. Sci., 49, 2139–2156.

Han, Q., Rossow, W. B. & Lacis, A. A. (1994). Near-global survey of effective droplet radii in liquid water clouds using ISCCP data, J. Clim., 7, 465– 497.

Han, Q., Rossow, W. B., Chou, J., Kuo, K.-S. & Welch, R. M. (1999). The effects of aspect ratio and surface roughness on satellite retrievals of ice cloud properties, J. Quant. Spectrosc. Radiat. Trans., 63, 559–583.

Held, I. M. &. Soden, B. J. (2000). Water vapor feedback and global warming. Annu. Rev. Energy Environ., 25, 441–475.

Kelley, M., Schmidt, G. A., Nazarenko, L. S., Bauer, S. E., Ruedy, R., Russell, G. L., et al. (2020). GISS−E2.1: Configurations and climatology. Journal of Advances in Modeling Earth Systems, 12, e2019MS002025. https://doi.org/10.1029/2019MS002025

Kinne, S. (2019). The MACv2 aerosol climatology, Tellus B: Chemical and Physical Meteorology, 71:1, 1-21, DOI: 10.1080/16000889.2019.1623639

Kopp, G., Lawrence, G. & Rottman, G. (2005). The Total Irradiance Monitor (TIM): Science Results, Sol. Phys., 230, 129-140.

Kramer, R. J., Matus, A. V., Soden, B. J., & L'Ecuyer, T. S. (2019). Observation-based radiative kernels from CloudSat/CALIPSO. Journal of Geophysical Research: Atmospheres, 124, 5431–5444. https://doi.org/10.1029/2018JD029021

Lacis, A.A., and Oinas, V. (1991). A description of the correlated k distributed method for modeling nongray gaseous absorption, thermal emission, and multiple scattering in vertically inhomogeneous atmospheres. J. Geophys. Res., 96, 9027-9063, doi:10.1029/90JD01945.

Manabe, S, (1969). Climate and the ocean circulation i-i. the atmospheric circulation and the effect of heat transfer by ocean currents, Monthly Weather Review, Vol. 97, No. 11, Nov. 1969, pp. 775-805.

Ohmura, A. (2014). The Development and the Present Status of Energy Balance Climatology, J. Meteor. Soc. Japan, Vol. 92, No. 4, pp. 245–285, 2014, DOI:10.2151/jmsj.2014-401.

Oreopoulos, L., Cho, N. & Lee, D. (2017). New insights about cloud vertical structure from CloudSat and CALIPSO observations, J. Geophys. Res. Atmos., 122, 9280–9300, doi:10.1002/2017JD026629.

Peixoto, J. P. & Oort, A. H. (1992). Physics of Climate, AIP, 520 pp.

Reynolds, R. W. (1988). A real-time global sea surface temperature analysis, J. Clim., 1, 75–86.

Roe, G. H, (2009). Feedbacks, timescales and seeing red. Annu. Rev. Earth. Planet. Sci. 37, 93–115.

Rossow, W. B., Walker, A. W., Bueschel, D. & Roiter, M. (1996). International Satellite Cloud Climatology Project (ISCCP) documentation of new cloud datasets, WMO/TD-737, 115 pp., World Clim. Res. Programme, Geneva, Feb.

Rossow, W. B. & Schiffer, R. A. (1999). Advances in understanding clouds from ISCCP, B. Am. Meteorol. Soc., 80, 2261–2288, https://doi.org/10.1175/1520-0477.

Rothman, L.S., Gordon, I.E.,,Babikov, Y., Barbe, A., Benner, Bernath, D. C., et al.(2013). The HITRAN2012 molecular spectroscopic database, J. Quantitative Spectroscopy & Radiative Transfer, 130(2013), 4-50.

Shell, K. M., Kiehl, J. T. & Shields, C. A. (2008). Using the radiative kernel technique to calculate climate feedbacks in NCAR's Community Atmospheric Model. J. Climate, 21, 2269–2282.

Schmidt, G.A., Ruedy, R., Hansen, J. E., Aleinov, I., Bell, N., Bauer, M., et al. (2006). Present day atmospheric simulations using GISS ModelE: Comparison to in-situ, satellite and reanalysis data. J. Climate, 19, 153-192, doi:10.1175/JCLI3612.1.

Shell, K. M., Kiehl, J. T., & Shields, C. A. (2008) Using the radiative kernel technique to calculate climate feedbacks in NCAR's Community Atmospheric Model. Journal of Climate, 21(10), 2269–2282. https://doi.org/10.1175/2007JCLI2044.1

Soden, B.J., Held, I. M., Colman, R., Shell, K. M., Kiehl, J. T. & Shields, C. A. (2008). Quantifying climate feedbacks using radiative kernels. J. Climate, 21, 3504–3520.

Stephens, G. L., Vane, D. G., Boain, R. J., Mace, G. G., Sassen, K., Wang, Z., et al. (2002). The CloudSat mission and the A-train: A new dimension of space-based observations of clouds and precipitation. Bull. Amer. Meteor. Soc., 83, 1771–1790.

Sun, Moguo, Doelling, D.R., Nguyen, L. T., Wilkins, J., & Mlynczak, P. (2019). A New CERES Cloud Type Based Flux Data Product: Algorithm, Validation and Application, American Geophysical Union, Fall Meeting 2019, abstract #A11B-07, Dec. 2019, Bibcode: 2019AGUFM.A11B..07S.

Wang, J., Rossow, W. B. & Zhang, Y.-C. (2000). Cloud vertical structure and its variations from 20-yr global rawinsonde dataset, J. Clim., 12, 3041–3056.

Wang, J. & Rossow, W. B. (1995). Determination of cloud vertical structure from upper-air observations. J. Appl. Meteor., 34, 2243–2258.

Wielicki, B. A., Barkstrom, B. R., Harrison, E. F., Lee, R. B., Smith, G. L. & Cooper, J. E. (1996)

Clouds and the Earth’s Radiant Energy System (CERES): An Earth Observing System experiment, Bull. Am. Meteorol. Soc., 77, 853– 868.

Winker, D. M., Pelon, J. R. & McCormick, M. P. (2003). The CALIPSO mission: Spaceborne lidar for observation of aerosols and clouds. Lidar Remote Sensing for Industry and Environment Monitoring III, U. N. Singh, T. Itabe, and Z. Liu, Eds., International Society for Optical Engineering (SPIE Proceedings, Vol. 4893), 1–11.

Young, A. H., Knapp, K. R., Inamdar, A., Hankins, W. & Rossow, W. B. (2018). The International Satellite Cloud Climatology Project H-Series climate data record product, Earth Syst. Sci. Data, 10, 583-593, https://doi.org/10.5194/essd-10-583-2018, 2018.

Yue, Q., Kahn, B. H., Fetzer, E.T., Schreier, M., Wong, S. Chen, X. & Huang, X. (2016). Observation−based longwave cloud radiative kernels derived from the A−Train. Journal of Climate, 29(6), 2023–2040. https://doi.org/10.1175/JCLI−D−15−0257.1

Zelinka, M. D., Klein, S. A. & Hartmann, D. L. (2012). Computing and partitioning cloud feedbacks using cloud property histograms. Part I: Cloud Radiative Kernels, J. Climate, 25, 3736–3754.

Zelinka, M. D., Myers, T. A., McCoy, D. T., Po-Chedley, S., Caldwell, P. M., Ceppi, P., et al., (2020a). Causes of higher climate sensitivity in CMIP6 models. Geophysical Research Letters, 47, e2019GL085782. https://doi.org/10.1029/2019GL085782

Zelinka, M. D., Myers, T.A., McCoy, D.T., Po-Chedley, S., Caldwell, P.M., Ceppi, P., Klein, S.A. & Taylor, K. E. (2020b) Supporting Information for "Causes of higher climate sensitivity in CMIP6 models" by Zelinka et al., 2020a (above).

Zhang, Y-C., Rossow, W.B., Lacis, A.A., Mishchenko, M.I. & Oinas, V. (2004). Calculation of radiative fluxes from the surface to top-of-atmosphere based on ISCCP and other global datasets: Refinements of the radiative transfer model and the input data. J.

Geophys. Res., 109, doi 10.1029/2003JD004457 (1-27 + 1-25), 2004.

Zhang, Y.-C., Rossow, W. B. & Stackhouse Jr., P. W. (2006). Comparison of different global information sources used in surface radiative flux calculation: Radiative properties of the near-surface atmosphere, J. Geophys. Res., 111, D13106, doi:10.1029/2005JD006873.

Zhang, Y.C., Rossow, W.B., Lacis, A.A. and Oinas, V. (2021). Calculation, evaluation and application of long-term, global radiative flux Datasets at ISCCP: Past and present. available (as "Zhang_etal_flux-cal_at-isccp_v4_2021.pdf") under "FH Documentation and Publications" at, https://isccp.giss.nasa.gov/projects/flux.html).

Zhou, C., Zelinka, M. D., Dessler, A. E. & Yang, P. (2013). An analysis of the short-term cloud feedback using MODIS data. J. Climate, 26, 4803–4815, https://doi.org/10.1175/JCLI-D-12-00547.1.

Table 1. The four cloud radiative kernel datasets used for comparison and evaluation.

CRK version	Derived from	Original spatial resolution	Original temporal resolution/coverage	τ x CTP indices	Comparison basis
FH	ISCCP-H + ISCCP-FH code	Global 110-km equal area	3-hourly for a year (of 2007)	7 x 7	12 monthly of τ-CTP histogram on global 280-km equal-area map (equivalent to 2° latitude x 2.5° longitude equal-angle map)
CS	MODIS-CERES Observation	Global 1° x 1°	Monthly for 12 months (of 2007)	6 x 7	
MZ	6-model mean states + Fu-Liou code	2° zonal*	Monthly for 12- month climatology	7 x 7	
OZ	ERA-Interim mean states + Fu-Liou code	2.5° zonal*	Monthly for 12- month climatology	7 x 7	

* In mapping zonal SW CRK to global map, the FH clear-sky surface albedo is used (the CERES surface clear-sky-albedo mapped has minor difference in tests so not used and shown) while zonal LW CRK is simply replicated to all longitudes (i.e., independent of longitudes).

Table 2. Summary of the statistics from comparison of monthly, global and 49- (or 42- for CS associated) bins TOA CRK in $Wm^{-2}\ \%^{-1}$†

X vs. Y CRKs	X mean	Y mean	Mean difference of (X – Y)	Stdv of (X – Y)	Correlation coefficient	Total equal-area grid cell number
LW Cloud Radiative Kernel						
FH vs MZ	0.514	0.556	-0.043	0.097	0.982	399612
FH vs OZ	0.514	0.549	-0.035	0.094	0.982	399612
MZ vs OZ	0.551	0.544	0.007	0.027	0.999	404348
FH vs CS	0.490	0.510	-0.021	0.176	0.922	260867
MZ vs CS	0.539	0.507	0.032	0.169	0.930	262546
OZ vs CS	0.529	0.507	0.021	0.170	0.928	262546
mean	0.523	0.529	-0.006	0.122	0.957	331589
modulus mean			0.027			
SW Cloud Radiative Kernel						
FH vs MZ	-0.957	-0.998	0.042	0.107	0.993	390251
FH vs OZ	-0.957	-0.991	0.034	0.104	0.993	390251
MZ vs OZ	-0.994	-0.986	-0.008	0.020	1.000	394230
FH vs CS	-0.966	-0.856	-0.110	0.172	0.978	260896
MZ vs CS	-1.010	-0.853	-0.157	0.190	0.977	262518
OZ vs CS	-1.000	-0.853	-0.147	0.187	0.977	262518
mean	-0.981	-0.923	-0.058	0.130	0.986	326777
modulus mean			0.083			
Net (total) Cloud Radiative Kernel						
FH vs MZ	-0.437	-0.436	-0.001	0.118	0.989	390251
FH vs OZ	-0.437	-0.437	0.000	0.115	0.990	390251
MZ vs OZ	-0.436	-0.437	0.001	0.030	0.999	394230
FH vs CS	-0.476	-0.346	-0.130	0.212	0.954	260863
MZ vs CS	-0.471	-0.346	-0.126	0.248	0.941	262484
OZ vs CS	-0.472	-0.346	-0.126	0.248	0.943	262484
mean	-0.455	-0.391	-0.064	0.162	0.969	326760
modulus mean			0.064			

† Each pair's statistics are averaged from their 12-monthly comparison for all bins and 250-km equal-area grid cells (8252 cells for a full map). X and Y are for the 6 possible combinations of the 4 sets of CRKs (Table 1). 'Stdv' is for standard deviation. The modulus (absolute) mean difference (Stdv) for 6 pairs are 0.027 (0.121), 0.083 (0.130) and 0.064 (0.162) $Wm^{-2}\ \%^{-1}$ for LW, SW and Net, respectively, translated to (bias-included) RMS of 0.124, 0.154 and 0.174 $Wm^{-2}\ \%^{-1}$ for LW, SW and Net, respectively. Because the same FU-Liou code is used for both the MZ and OZ CRKs' calculation, they are not completely independent and the above RMS estimates may be underestimated. When the OZ CRKs are removed, the completely independent 3-set CRKs' RMS is increase by ~20% (Table S1 in Supporting Information, SI).

Table 3. Ten global CFMIP1 models used for 2 x CO_2 cloud fraction change experiment†

No.	GCM Climate Models for CMIP1	Abbrev.
1	CCSM3.0* National Center for Atmospheric Research, USA	‘n3’
2	HadSM3 Hadley Centre for Climate Prediction and Research/Met Office, UK	‘u3’
3	GFDL MLM2.1* NOAA/Geophysical Fluid Dynamics Laboratory, USA	‘gf’
4	IPSL CM4* Institute Pierre Simon Laplace, France	‘ip’
5	BMRC1* Bureau of Meteorology Research Centre, Australia	‘bm’
6	MIROC(hires)* Center for Climate System Research, The University of Tokyo	‘mh’
7	MIROC(lowres) Center for Climate System Research, The University of Tokyo	‘ml’
8	UIUC University of Illinois at Urbana–Champaign, USA	‘ui’
9	HadGSM1 Hadley Centre for Climate Prediction and Research/Met Office, United Kingdom	‘ul’
10	HadSM4 Hadley Centre for Climate Prediction and Research/Met Office, United Kingdom	‘u4’

†Z2012’s Table 1 lists 12 CFMIP1 models, of which only 11 models (excluding MPI ECHAM5) were actually used in Z2012. Of the 11 models, one (AGCM4) has a quality issue so we do not use it (personal communication with Dr. Zelinka). Asterisks denote the 5 models whose atmospheric temperature and specific humidity profiles were unavailable and not used for Z2012’s CRKs’ calculation. The last column is the abbreviations of the ten models, used in Table S2 in Supporting Information (SI).

Table 4. Uncertainty budget for regional, monthly and bin-mean for TOA cloud feedback, based on RMS of the 4 TOA cloud radiative kernel (Table 2) and the 10 GCM’s (normalized) cloud fraction change (CFC) in 2 x CO_2 experiments (Table S2 in SI)†.

CRK from	CRK uncertainty	Mean CFC	CRK uncertainty contribution	Mean CRK	CFC uncertainty	CFC uncertainty contribution	Cloud feedback uncertainty
	δk	ΔC	δk ·ΔC	k	δ(ΔC)	k ·δ(ΔC)	δk ·ΔC + k · δ(ΔC)
LW	0.124	0.010	0.00123	0.529	0.332	0.176	0.177
SW	0.154	0.010	0.00154	0.952	0.332	0.316	0.318
Net	0.174	0.010	0.00174	0.423	0.332	0.140	0.142

† k is k_{X_i} for CRK and ΔC is $\frac{dX_i}{dT_s}$ for rate of cloud fraction change with respective to surface air temperature (normalization). Uncertainty of CRK (δk) and CFC [δ(ΔC)] are RMS from Table 2 and S2 (in SI), respectively. Mean k and mean ΔC are the average of the module X and Y from Table 2 and Table S2 (in SI), respectively. CRK is in $Wm^{-2}\ \%^{-1}$, CFC in $\%K^{-1}$ and cloud feedback in $Wm^{-2}\ K^{-1}$.

Table 5. Minimum and maximum values as range of total cloud feedback (sum of 49 bins) from double CO_2 experiments for global and annual mean of the 10 models using FH CRKs and their ensemble mean (also shown in the title of Fig. 6) in $W/m^{-2}\ K^{-1}$ for TOA, SFC and ATM†

	TOA			SFC			ATM		
	Min	Max	Ensemble	Min	Max	Ensemble	Min	Max	Ensemble
LW	-0.11	0.68	0.20	-0.22	0.00	-0.10	-0.10	0.81	0.30
SW	-0.26	0.86	0.33	-0.21	0.94	0.36	-0.08	0.00	-0.04
Net	0.16	0.89	0.53	-0.34	0.72	0.27	-0.10	0.76	0.26

†Z2012's range of total TOA global mean cloud feedback are -0.13 to 0.69, -0.18 to 0.93 and 0.16 to 0.94 $Wm^{-2}\ K^{-1}$ for LW, SW and Net, respectively, based on 11 models, of which, 10 models' are shown here. Their ensemble values are 0.21, 0.37 and 0.57 $Wm^{-2}\ K^{-1}$, for TOA LW, SW and Net, respectively. The small differences between Z2012's and this study are caused by both model number (11 vs. 10) and CRK difference. The (normalized) CFC range is -0.882 to -0.0002 with ensemble value of -0.47 $\%K^{-1}$ from this study compared Z2012's -0.91 to -0.02 with ensemble value of -0.46 $\%K^{-1}$.

Table 6. Global average of cloud feedback contributions (in $Wm^{-2}\ K^{-1}$), partitioned to high, middle and low clouds, and thin-, medium- and thick-τ clouds, respectively†.

a. Partitioned for high, middle and low clouds									
Clouds	LW			SW			NET		
	TOA	SFC	ATM	TOA	SFC	ATM	TOA	SFC	ATM
Total	0.20	-0.09	0.29	0.32	0.35	-0.03	0.52	0.26	0.26
High	0.30	0.04	0.27	-0.18	-0.19	0.01	0.12	-0.15	0.27
Middle	-0.09	-0.06	-0.03	0.24	0.24	-0.01	0.15	0.18	-0.04
Low	-0.01	-0.07	0.06	0.26	0.29	-0.03	0.25	0.22	0.02
b. Partitioned for thin-, medium- and thick-τ clouds									
τ	LW			SW			NET		
	TOA	SFC	ATM	TOA	SFC	ATM	TOA	SFC	ATM
Total	0.20	-0.09	0.29	0.32	0.35	-0.03	0.52	0.26	0.26
Thin	-0.00	-0.10	0.10	0.04	0.05	-0.01	0.04	-0.05	0.09
Medium	0.04	-0.10	0.14	0.30	0.33	-0.04	0.34	0.23	0.11
Thick	0.17	0.11	0.05	-0.03	-0.03	0.01	0.14	0.08	0.06

†The total global average is identical for the two different partitions.

AGU PUBLICATIONS

Journal of Geophysical Research

Supporting Information for

Top-of-atmosphere, surface and atmospheric cloud radiative kernels based on ISCCP-H datasets: Method and Evaluation

Yuanchong Zhang[1,2], Zhonghai Jin[2] and Monika Sikand[3]

[1]SciSpace LLC

[2]NASA Goddard Institute for Space Studies, New York, NY 10025, USA

[3]Deptment of Engineering, Physics, and Technology, Bronx Community College, CUNY. NY, 10453

Contents of this file

Tables S1 to S3

Introduction

Table 2 in Main text is based on the statistical comparison for six pairs of all possible combinations of the four cloud radiative kernel (CRK) datasets, FH, CS, MZ and OZ. However, the MZ and OZ are calculated using the same Fu-Liou radiation code (but with different input of mean climate states) so that the four CRK datasets may be not completely independent. To address this issue, we remove OZ CRK datasets and then do the same comparison but for three pairs of all possible combinations of the three CRK datasets (FH, CS and MZ). Table S1 shows that RMS values are increased by ~20% based on the new comparison, which should be more objective than those from Table 2 in Main text since the three CRK datasets are now completely independent of each other.

Using the same statistical comparison as Table S1 (or Table 2 in main text), we have also made comparison for (normalized) cloud fraction changes (CFC) for 45 pairs of all possible combinations of the 10 CFMP1 models for 1 x CO2 to 2 x CO2 experiments. The results are shown in Table S2, which is too large to be presented in Main text. For convenience, we have copied Table 3 in Main text as Table S3 here for list of all the 10 models.

Table S1.

Summary of the statistics from comparison of monthly, global and 49- (or 42- for CERES associated) bins TOA for cloud radiative kernel (CRK) in Wm^{-2} $\%^{-1}$

X vs. Y CRKs	X mean	Y mean	Mean difference of (X – Y)	Stdv of (X – Y)	Correlation coefficient	Total equal-area grid cell number
LW Cloud Radiative Kernel						
FH vs MZ	0.514	0.556	-0.043	0.097	0.982	399612
FH vs CS	0.490	0.510	-0.021	0.176	0.922	260867
MZ vs CS	0.539	0.507	0.032	0.169	0.930	262546
mean	0.514	0.525	-0.011	0.147	0.945	307675
modulus mean			0.032			
SW Cloud Radiative Kernel						
FH vs MZ	-0.957	-0.998	0.042	0.107	0.993	390251
FH vs CS	-0.966	-0.856	-0.110	0.172	0.978	260896
MZ vs CS	-1.043	-0.853	-0.190	0.180	0.983	262576
mean	-0.988	-0.902	-0.086	0.153	0.985	304574
modulus mean			0.114			
Net (total) Cloud Radiative Kernel						
FH vs MZ	-0.437	-0.436	-0.001	0.118	0.989	390251
FH vs CS	-0.476	-0.346	-0.130	0.212	0.954	260863
MZ vs CS	-0.504	-0.345	-0.159	0.233	0.954	262542
mean	-0.472	-0.376	-0.097	0.188	0.966	304552
modulus mean			0.097			

† Each pair's statistics are averaged from their 12-monthly comparison for all bins and 250-km equal-area grid cells (8252 cells for a full map). X and Y are for the 3 possible combinations of the 3 sets of CRKs. 'Stdv' is for standard deviation. The modulus (absolute) mean difference (Stdv) for 3 pairs are 0.032 (0.147), 0.114 (0.153) and 0.097 (0.188) Wm^{-2} $\%^{-1}$ for LW, SW and Net, respectively, translated to (bias-included) RMS 0.150, 0.191 and 0.212 Wm^{-2} $\%^{-1}$ for LW, SW and Net, respectively. The RMS estimates is about 20% larger than those in Table 2 in main text (based on 6 pairs, all the possible combinations for 4 CRK sets), and should be more objective (cf. Table 2 in Main text).

Table S2.

Summary of the statistics from comparison of monthly, global and 49- (or 42- for CERES associated) bins for cloud fraction change (CFC) in %/K from 1 x CO2 to 2

x CO2 model runs, normalized by individual model's surface air temperature changes†

X vs. Y CFC	X mean	Y mean	Mean difference of (X – Y)	Stdv	Correlation coefficient	Total equal-area box number
n3 vs u3	-0.0004	-0.0088	0.008	0.335	0.103	397639
n3 vs gf	-0.0004	-0.0096	0.009	0.345	0.120	398015
n3 vs ip	-0.0004	-0.0158	0.015	0.357	0.173	397794
n3 vs bm	-0.0004	-0.0065	0.006	0.307	0.034	398015
n3 vs mh	-0.0004	-0.0185	0.018	0.326	0.151	397770
n3 vs ml	-0.0004	-0.0139	0.014	0.404	0.051	397770
n3 vs ui	-0.0004	-0.0112	0.011	0.435	0.061	397819
n3 vs u1	-0.0004	-0.0087	0.008	0.306	0.068	398015
n3 vs u4	-0.0004	-0.0064	0.006	0.295	0.100	397639
u3 vs gf	-0.0087	-0.0096	0.001	0.307	0.222	397680
u3 vs ip	-0.0087	-0.0158	0.007	0.351	0.122	397664
u3 vs bm	-0.0087	-0.0065	-0.002	0.282	0.047	397884
u3 vs mh	-0.0088	-0.0186	0.010	0.301	0.179	397459
u3 vs ml	-0.0088	-0.0140	0.005	0.365	0.158	397459
u3 vs ui	-0.0087	-0.0112	0.002	0.401	0.152	397680
u3 vs u1	-0.0087	-0.0087	-0.000	0.274	0.130	397884
u3 vs u4	-0.0087	-0.0063	-0.002	0.251	0.241	397884
gf vs ip	-0.0096	-0.0158	0.006	0.360	0.139	397835
gf vs bm	-0.0096	-0.0065	-0.003	0.308	0.046	398174
gf vs mh	-0.0097	-0.0185	0.009	0.293	0.247	397823
gf vs ml	-0.0097	-0.0139	0.004	0.360	0.199	397823
gf vs ui	-0.0096	-0.0112	0.002	0.423	0.103	397941
gf vs u1	-0.0096	-0.0087	-0.001	0.290	0.186	398174
gf vs u4	-0.0096	-0.0064	-0.003	0.272	0.199	397680
ip vs bm	-0.0158	-0.0065	-0.009	0.330	0.037	397860
ip vs mh	-0.0158	-0.0186	0.003	0.356	0.098	397562
ip vs ml	-0.0158	-0.0139	-0.002	0.398	0.154	397562
ip vs ui	-0.0158	-0.0112	-0.005	0.454	0.045	397696
ip vs u1	-0.0158	-0.0087	-0.007	0.305	0.212	397835
ip vs u4	-0.0158	-0.0064	-0.009	0.304	0.194	397664
bm vs mh	-0.0065	-0.0185	0.012	0.281	0.056	398015
bm vs ml	-0.0065	-0.0139	0.007	0.355	0.044	398015
bm vs ui	-0.0065	-0.0112	0.005	0.395	0.019	399158
bm vs u1	-0.0065	-0.0087	0.002	0.235	0.053	398627
bm vs u4	-0.0065	-0.0063	-0.000	0.221	0.089	397884
mh vs ml	-0.0185	-0.0139	-0.005	0.323	0.359	398015
mh vs ui	-0.0185	-0.0112	-0.007	0.391	0.195	397843
mh vs u1	-0.0185	-0.0087	-0.010	0.279	0.098	398015
mh vs u4	-0.0186	-0.0064	-0.012	0.262	0.162	397459
ml vs ui	-0.0139	-0.0112	-0.003	0.457	0.104	397843
ml vs u1	-0.0139	-0.0087	-0.005	0.331	0.208	398015
ml vs u4	-0.0140	-0.0064	-0.008	0.328	0.194	397459
ui vs u1	-0.0112	-0.0087	-0.002	0.398	0.020	398301
ui vs u4	-0.0112	-0.0064	-0.005	0.391	0.036	397680
u1 vs u4	-0.0087	-0.0063	-0.002	0.184	0.396	397884
mean	-0.0092	-0.0107	0.002	0.332	0.133	397865
modulus mean			0.004			

†Each pair's statistics are averaged from their 12-monthly comparison for all bins and 250-km equal-area grid cells (8252 cells for a full global map). The modulus mean of 45 pairs' mean difference (Stdv) is 0.004 (0.332), % K^{-1} translated to (bias-included) RMS of 0.332.The versions of the 45 pairs are referred to Table S3.

Table S3.

Ten global CFMIP1 models used for 2 x CO_2 cloud fraction change experiment†

No.	GCM Climate Models	Abbrev.
1	CCSM3.0* National Center for Atmospheric Research, USA	‘n3’
2	HadSM3 Hadley Centre for Climate Prediction and Research/Met Office, UK	‘u3’
3	GFDL MLM2.1* NOAA/Geophysical Fluid Dynamics Laboratory, USA	‘gf’
4	IPSL CM4* Institut Pierre Simon Laplace, France	‘ip’
5	BMRC1* Bureau of Meteorology Research Centre, Australia	‘bm’
6	MIROC(hires)* Center for Climate System Research, The University of Tokyo	‘mh’
7	MIROC(lowres) Center for Climate System Research, The University of Tokyo	‘ml’
8	UIUC University of Illinois at Urbana–Champaign, USA	‘ui’
9	HadGSM1 Hadley Centre for Climate Prediction and Research/Met Office, United Kingdom	‘ul’
10	HadSM4 Hadley Centre for Climate Prediction and Research/Met Office, United Kingdom	‘u4’

†Z2012’s Table 1 lists 12 CFMIP1 models, of which only 11 models (excluding MPI ECHAM5) were actually used in Z2012. Of the 11 models, one (AGCM4) has a quality issue so we do not use it (personal communication with Dr. Zelinka). Asterisks denote the 5 models whose atmospheric temperature and specific humidity profiles were unavailable and not used for Z2012’s CRKs’ calculation. The last column is the abbreviations of the ten models, used in Table S2 in Supporting Information (SI).

.